Received: 19 July 2019 | Revised: 4 July 2020 | Accepted: 1 August 2020

DOI: 10.1002/navi.395

ORIGINAL ARTICLE

WILEY ION

Performance comparison of time-of-arrival estimation techniques for LTE signals in realistic multipath propagation channels

Pai Wang | **Y. Jade Morton**

Colorado Center for Astrodynamics Research, Smead Aerospace Engineering Sciences Department, University of Colorado Boulder, Boulder, CO 80309, USA

Correspondence
P. Wang, Smead Aerospace Engineering Sciences Department, University of Colorado Boulder, Boulder, CO 80303, USA.
Email: wendywang.bit@gmail.com

Abstract

Long term evolution (LTE) signals have the potential for use in positioning, especially in challenging environments. The time-of-arrival (TOA)-based technique supported by LTE is attractive due to its high positioning accuracy. However, it is vulnerable to multipath propagation effects in typical LTE channels. This paper will summarize several existing advanced TOA estimators for LTE signals, i.e., first peak detection, information theoretic criteria, super-resolution algorithm, and delay-lock loop (DLL). Later, the paper will evaluate the TOA estimation performances of these techniques with multipath propagation effects and varying signal conditions using simulations. For the DLL, the multipath error envelope metric is assessed for different signal bandwidths. The root mean square errors of the TOA estimations are compared to evaluate suitable TOA estimators under various conditions. Finally, some other performance characteristics of these techniques are also discussed.

KEYWORDS
long term evolution, multipath propagation channel, time-of-arrival estimation

1 | INTRODUCTION

Improvements in the precision of positioning and navigation have been motivated by numerous location-based applications. These would include vehicle navigation, aviation navigation, enhanced 911 service, location-aware communication, and asset tracking, which all demand reliable and accurate location information. Global Navigation Satellite System (GNSS) receivers are widely adopted to provide positioning and navigation results, and they generally offer a high positioning accuracy in open-sky areas (Parkinson et al., 1996). However, in challenging environments, such as indoors or in urban canyons, the poor reception of L-band satellite signals makes them much less effective. Therefore, positioning and navigation in challenging environments cannot solely rely on GNSS signals.

Long term evolution (LTE)-based positioning has emerged as a viable alternative or augmentation to GNSS for indoor/urban navigation (Cherian & Rudrapatna, 2013; Dammann et al., 2011; Mensing et al., 2010). The LTE standard specifies a variety of positioning methods, e.g., assisted GNSS, enhanced cell ID, observed time-difference-of-arrival (OTDOA), and uplink TDOA. An extensive survey of these LTE location technologies can be found in Cherian and Rudrapatna (2013) and del Peral-Rosado et al. (2017). Much effort has been devoted to

methods that rely on time-of-arrival (TOA) measurements. Performance of the TOA-based LTE positioning method and the impact of various factors on it have been analyzed through theoretical analysis, computer simulations, and experimental campaigns. For example, Shamaei et al. (2017) evaluated and compared the positioning capabilities of two LTE downlink signals. Several realistic propagation channel models adopted by the LTE standard were used for evaluating the TOA error distribution obtained with the conventional approach (del Peral-Rosado et al., 2012c). A software-defined radio (SDR) receiver on two low-cost hardware platforms was tested by experiments analyzing the received signal power and positioning accuracy (del Peral-Rosado, Parro-Jiménez, et al., 2014). The performance for a range of LTE signal bandwidths was discussed in del Peral-Rosado, López-Salcedo, et al. (2014) and Xu et al. (2016). A more detailed survey of the existing work on assessing the LTE positioning capabilities based on TOA measurements will be given in Section 2 of this paper.

Studies show that the positioning reference signal (PRS) and cell-specific reference signal (CRS) transmitted in the LTE downlink physical layer both offer promising positioning performances in environments without severe multipath (del Peral-Rosado et al., 2012b; Shamaei et al., 2017). As pointed out by Shamaei and Kassas (2018), there are a few issues that arise from the PRS-based positioning due to its optional transmission, network-based positioning, and the exploitation of signals from a single cellular provider. Consequently, this paper focuses on the CRS-based positioning. As TOA estimation is a special problem of channel estimation, a popular CRS TOA estimation technique is based on detecting the peak of the channel impulse response (CIR) (Knutti et al., 2015). Nevertheless, the multipath propagation effect remains as one of the main error sources in the TOA estimations obtained with this conventional approach, especially for indoor and urban navigation (del Peral-Rosado et al., 2012c). Recently, several advanced techniques using channel estimation results have been developed to address the TOA estimation accuracy issue in multipath environments. To the best of the authors' knowledge, there has not been a thorough review of these advanced TOA estimators and their performance evaluation for multipath propagation channels under varying signal conditions.

This paper analyzes several of the advanced TOA estimation techniques for the LTE CRS (Driusso et al., 2017): the first peak detection (FPD) (Dardari et al., 2008; Guvenc & Sahinoglu, 2005), information theoretic criteria (ITC) (Giorgetti & Chiani, 2013), super-resolution algorithm (SRA) (Li & Pahlavan, 2004), and delay-lock loop (DLL) (Shamaei & Kassas, 2018). Several LTE tapped-delay line (TDL) channel models, such as the Extended Pedestrian A (EPA), Extended Vehicular A (EVA), and Extended Typical Urban (ETU), are implemented to simulate multipath propagation effects for the TOA estimation performance assessment (3GPP, 2019b). The TOA estimation errors generated by the algorithms under evaluation are obtained for simulated propagation channel models at a wide range of signal-to-noise power ratio (SNR) values and different signal bandwidths. The TOA error analysis results clearly indicate the strengths and weaknesses of the estimation techniques. These results can be used to guide the selection of suitable TOA estimators based on the propagation channels and specific LTE signal conditions.

The rest of the paper is organized as follows. Section 2 reviews the performance of the TOA-based positioning using LTE signals. Section 3 describes the LTE frame structure and the mathematical models of multipath propagation channels. Section 4 covers the channel estimation process in the LTE receiver. Section 5 describes each advanced TOA estimator with performance results evaluated under different channel types and signal conditions. Section 6 offers a comparison and discussion for the considered algorithms. Section 7 provides a summary.

2 | REVIEW OF PERFORMANCE ANALYSIS OF THE TOA-BASED POSITIONING USING LTE SIGNALS

This section provides a review of the existing literature on the TOA-based positioning and performance evaluations using LTE signals. Either downlink signals transmitted by multiple eNodeBs or uplink signals transmitted by user equipment (UE) can be exploited for positioning (Cherian & Rudrapatna, 2013). Here, the downlink LTE signals are used to produce the TOA measurements. In the following discussion, we mainly focus on the TOA estimation algorithm, specific LTE downlink signal, and how to conduct performance analysis in each literature.

2.1 | Theoretical bound analysis

The theoretical Cramer-Rao lower bound (CRLB) is commonly used to indicate the maximum achievable accuracy of an unbiased estimator under moderate to high SNR conditions. In Wang and Fattouche (2010), the CRLB for the TOA estimation with generic orthogonal frequency division multiplexing (OFDM) signals in an additive white Gaussian noise (AWGN) environment was derived based on an approximation of the mean square bandwidth of the OFDM signal and was compared to that of a pseudo-random noise (PRN) signal. It was proven

that the required SNR of the OFDM signal is 4.8 dB lower than the PRN signal to achieve the same ranging accuracy in the asymptotic region. In the presence of AWGN plus a zero-mean complex Gaussian process modeled interference, a closed-form CRLB expression of the TOA estimation was studied for OFDM systems (Karisan et al., 2011). The CRLB and Ziv-Zakai bound for characterizing the TOA estimation performance of realistically modeled OFDM signals, e.g., those in the third-generation partnership project (3GPP) LTE specification, in the AWGN channel were derived in Driusso et al. (2014). These bounds were then used to analyze the TOA estimation behavior in both the asymptotic and threshold regions considering two sets of subcarrier power distributions. The analysis revealed the specific strategy for subcarrier power distribution to achieve a satisfactory asymptotic or threshold performance. In del Peral-Rosado et al. (2012b) and Gentner, Sand, et al. (2012), the CRLB expression in Wang and Fattouche (2010) was extended for analyzing the theoretical limits of the TOA estimation accuracy with LTE pilot signals. The impact of inter-cell interference in the LTE network and the effectiveness of inter-cell interference coordination techniques were also analyzed in del Peral-Rosado et al. (2012b) by computing the equivalent signal-to-interference plus noise ratio in the AWGN channel. A more rigorous CRLB for the TOA estimation with LTE signals in the AWGN channel was provided in Xu et al. (2016) without exploiting the approximation of the mean square bandwidth. A comparison of the CRLBs derived from several LTE pilots or a combination of these pilots was given.

For multipath channels, the closed-form expression of the Fisher information matrix for all the channel parameter estimations in OFDM systems was derived (Wang et al., 2013). Based on this, the effects of signal and channel parameters on the ranging accuracy were then quantified in multipath channels. Researchers in del Peral-Rosado et al. (2018) calculated the CRLBs for several channel estimation models, i.e., the periodic-tap model, hybrid-tap model, and arbitrary-tap model. These theoretical expressions can be used to deduce the achievable accuracy of several joint maximum likelihood (ML) time-delay and channel estimators developed from these channel estimation models in static multipath channels. The CRLBs for the TOA estimation using the PRS with 5G radio access were derived considering a multipath channel with AWGN, carrier frequency offset, and Wiener phase noise (Luan, 2017). The effects of flexible bandwidth, subcarrier spacing, and power allocation on the TOA estimation accuracy were investigated to guide the PRS redesign for 5G-based positioning. However, it should be noted that no theoretical CRLB exists for varying multipath channels (Xu et al., 2016).

2.2 | Error modeling

In general, the TOA measurements may be corrupted by many error sources, such as thermal noise, non-line-of-sight (NLOS) propagation, multipath effects, clock drift, and receiver motion. Empirical or theoretical error models for the TOA or TDOA measurements in LTE systems have been established for a variety of scenarios. A measurement campaign was performed in an indoor scenario (Gentner, Muñoz, et al., 2012) during which the receiver generated the TOA estimation by detecting the first correlation peak above a heuristic threshold using the synchronization signals with scattered pilots. An approximate Gaussian distributed TDOA error model was then built through statistical analysis. In Kong and Kim (2016), the analytical expressions for the probability density function (PDF) of the TOA errors caused by the scattering environment, multipath effects, and thermal noise were derived, respectively. Note that the TOA estimation was related to the resolved first arrival path measured from the PRS. A Gaussian scatter distribution model was assumed and both the Rician and Rayleigh channels were considered for representing outdoor multipath environments. The overall TOA and TDOA error distributions were then obtained by integrating all the error PDFs due to a variety of factors. Specifically, for a low LTE signal bandwidth, the TOA errors introduced by multipath channels were modeled as a skew-t distribution (Müller et al., 2016). The parameters of the skew-t distribution were obtained by fitting training data of the TOA errors obtained from several types of TDL channel models. It was demonstrated that the application of these error models in the positioning algorithm yielded an improved positioning accuracy.

2.3 | Computer simulations

Various channel models have been specified by the 3GPP to characterize the multipath fading propagation conditions present in typical LTE channels. Through a large number of channel realizations, computer simulations can be implemented to statistically test the LTE positioning capabilities in complex propagation channels.

It was not until the end of 2009 that the dedicated PRS devoted to the OTDOA technique had been introduced by the 3GPP in Release 9 (3GPP, 2010; Sven, 2014). Before that, some pioneering work was done using synchronization signals and scattered pilot signals in the 3GPP LTE. In Mensing et al. (2007), two symbol timing synchronization approaches for OFDM systems, i.e., the Schmidl-Cox algorithm and the Minn algorithm, were examined with respect to their positioning capabilities using the scattered pilot signals in the WINNER C2 wide area channel model.

To combat the inter-cell interference, an interference cancellation scheme combined with the conventional correlation-based timing estimation algorithm was developed in Mensing et al. (2009b). Mensing et al. (2009a) further integrated a data feedback approach using already decided data symbols into the method in Mensing et al. (2009b) to overcome the limited number of pilot symbols. These two algorithms were tested with the second synchronization signal (SSS) considering both an AWGN channel and a typical urban multipath channel. The authors in Benedetto et al. (2011) applied a parabolic interpolation around the maximum of the correlation function obtained with the primary synchronization signal (PSS) to refine the TOA estimation with performance evaluation in an AWGN channel. However, this algorithm has been shown to be vulnerable to harsh multipath conditions where the first arriving path is severely attenuated and a few close-in multipaths exist (Gadka et al., 2019).

The correlation-based peak or FPD algorithms are currently widely used for LTE-based positioning. In del Peral-Rosado et al. (2012c), the accuracy of the conventional ML estimator based on the time-domain correlation results using the PRS was evaluated for severe multipath scenarios represented by the TDL channel models and geometric-based stochastic channel models. The multipath resolution capabilities for a range of LTE PRS bandwidths were also characterized. The effect of multipath on the first peak estimator using the PRS was then assessed in del Peral-Rosado et al. (2012a) for the TDL channel models in a noisy environment. In addition, the joint impact of inter-cell interference and multipath was also analyzed. Another first arriving path detection method with two threshold settings on the basis of the time-domain correlation results was proposed in Huang and Xu (2013) and Xu et al. (2016). Their estimation performances with the PRS or CRS were analyzed using simulations for the TDL channel models. In Rydén et al. (2015), the horizontal and vertical indoor positioning performances of the LTE OTDOA technique using the first peak-based TOA estimator were evaluated with 3D multiple-input, multiple-output (MIMO) channel models. Two simulation scenarios of outdoor-only and outdoor-indoor network deployments were under consideration. The results indicated that the indoor LTE positioning accuracy could be enhanced by deploying more small cells indoors and outdoors.

Some other TOA estimation algorithms have also emerged for coping with LTE signals. In Panchetti et al. (2013), the phase information of the cross-correlation product between the channel frequency response (CFR) estimations obtained at two adjacent OFDM symbols containing the PRS was extracted for the TOA estimation. Performance analysis of this approach in both the AWGN and TDL multipath channels was carried out by simulations. According to a hybrid-tap model, which includes equally spaced taps plus an arbitrary tap within the first two taps, a joint ML time-delay and channel estimation technique was proposed by solving the corresponding two-dimensional optimization problem (del Peral-Rosado, Parro-Jiménez, et al., 2014). The performance improvement of this two-dimensional estimator over the one-dimensional one based on a periodic-tap model using the PRS was demonstrated by simulations for a combined multipath propagation and AWGN channel. An iterative TOA estimation algorithm, which excluded the contribution of already detected paths in the CIR at each iteration, was developed in Rydén et al. (2016) to overcome the poor accuracy and complex parameter tuning in the threshold-based noniterative method. The performance was evaluated using an International Telecommunication Union (ITU) Macro 3D channel model and outdoor-indoor network deployment scenario. Chen et al. proposed a novel OTDOA technique for three-dimensional positioning in LTE systems (Chen & Wu, 2016). A compressive sensing channel estimation method exploiting the inherent sparsity of the CIR was used for the TOA estimation. The positioning performance was assessed in a simulation scenario considering the EPA and ETU channel models. Simulation results showed that 90% of the position errors provided by the proposed scheme were less than 7 m. The estimation of signal parameters by the rotational invariance technique (ESPRIT) was used in Dan et al. (2018) for joint TOA and direction of arrival (DOA) estimation with the CRS considering a UE equipped with two antennas. The positioning performance was only evaluated for static multipath channels.

2.4 | Experiment testing

Another straightforward way is to conduct experiments for evaluating the LTE positioning capabilities. The common FPD approach was employed in Medbo et al. (2009) for producing the ranging measurements, which detected the first arriving signal by the first occurrence of a signal level above a −30 dB detection threshold relative to the strongest peak in the power delay profile (PDP). Provided with the real channel data measured by a channel sounder using the PRS, the received signal strengths and positioning errors were analyzed. For the LTE-based indoor positioning system developed in Gentner, Munoz, et al. (2012), the TOA was estimated by detecting a correlation peak before the maximum peak with a threshold of 8 dB below the maximum peak. The ranging and positioning accuracy obtained with this system was evaluated through a measurement campaign for an outdoor to indoor scenario. Shamaei et al. developed an SDR LTE positioning receiver using four

main stages for timing estimation: cell acquisition, system information extraction, signal tracking, and timing information extraction (Shamaei et al., 2018b). At the last stage, the TOA was measured from the CRS by a first peak estimator, which computes an adaptive threshold according to the varying noise level and a constant false alarm rate. The positioning performance obtained with this SDR receiver was examined by field tests conducted with an unmanned aerial vehicle (UAV) and a ground vehicle. The authors in Gadka et al. (2019) proposed two peak detection strategies for low and high bandwidths of LTE downlink signals. Simulated and experimental results were used for obtaining an adaptive threshold criterion based on SNR values. The estimation accuracy was assessed through a measurement campaign carried out based on a real LTE network in an urban scenario. The LTE-based navigation performance was tested using an LTE SDR made up of a universal software radio peripheral (USRP) B200mini radio front-end and an open source software implementation of a UE (Ikhtiari, 2019). Only the cell acquisition approach with the PSS and SSS was used to estimate the TOA. Through the experiments conducted in both mild and severe multipath conditions, the authors claimed that the biggest contributor of positioning error was the UE clock drift. A few solutions for combating the clock drift issue were discussed.

Another category of LTE signal TOA estimator makes use of the SRA, e.g., ESPRIT, based on the channel frequency measurements (Li & Pahlavan, 2004). In Driusso et al. (2017, 2016), a TOA estimation algorithm, named the ESPRIT and Kalman filter for time-of-Arrival Tracking (EKAT), using the CRS, was proposed to increase the robustness to multipath effects. Signal combination in multiple domains, i.e., time, frequency, spatial, and cell ID domains, was adopted for performance enhancement. Live data of commercial LTE signals were gathered in different propagation environments to demonstrate the advantage of the ranging accuracy provided by the proposed algorithm over other existing methods in Benedetto et al. (2011), Dardari et al. (2008), Giorgetti and Chiani (2013), and Knutti et al. (2015). The EKAT algorithm was also used in Pittino et al. (2017) to evaluate the positioning performance with real collected LTE data in both outdoor and indoor testing environments.

One disadvantage of the SRA is the high computational cost, which motivates the application of the computationally efficient closed-loop approaches. The SDR LTE positioning receivers presented in del Peral-Rosado, Parro-Jiménez, et al. (2014) and del Peral-Rosado et al. (2013) implemented a tracking architecture based on a DLL and a phase-lock loop (PLL) using the CRS for time and frequency synchronization. They employed a Fitz estimator and a ML estimator for TOA estimation in the DLL, respectively. An experimental testbed based on an emulated LTE network with a static UE was built. The real LTE signals generated in the testbed were captured by a USRP platform for performance validation of the SDR receiver in del Peral-Rosado et al. (2013). The positioning results obtained from the SDR receiver in del Peral-Rosado, Parro-Jiménez, et al. (2014) with two low-cost hardware platforms, i.e., a USRP platform and a digital video broadcasting-terrestrial (DVB-T) dongle, were compared. In Shamaei et al. (2018a), the authors assessed the ranging accuracy for only using the signal tracking stage based on the SSS in Shamaei et al. (2018b) by experimental results of a ground vehicle. Field tests were conducted in Shamaei et al. (2017) to compare the LTE positioning accuracy obtained with the CRS-based receiver (Shamaei et al., 2018b) and the SSS-based receiver (Shamaei et al., 2018a). In Shamaei and Kassas (2018), another SDR LTE positioning receiver architecture was presented with two main stages, i.e., acquisition and tracking. Provided with the initial TOA estimation from the ESPRIT algorithm, a PLL-aided DLL was developed to track the LTE CRS. The effectiveness of this SDR receiver was verified by experiments on a ground vehicle in an urban environment. The pseudorange accuracy of the two SDR receivers proposed by Shamaei and Kassas (2018) and Shamaei et al. (2018b) was also compared with several state-of-the-art algorithms.

In addition, an iterative TOA estimation algorithm with multi-access interference mitigation using the PSS was developed and examined by a generic OFDM-based positioning testbed (Staudinger & Gentner, 2011; Staudinger et al., 2011). With the same collected data as in Driusso et al. (2017), the performance of another TOA estimator aiming at rejecting NLOS measurements was evaluated in Knutti et al. (2015). Several peaks exceeding a predefined threshold were detected in the CIR estimation obtained from the CRS. The TOA measurement would be discarded if the first peak is not the highest among all detected peaks. Laboratory experiments were carried out in del Peral-Rosado et al. (2018) to evaluate the ranging performances of several joint ML time-delay and channel estimators. A controlled scenario only with the effects of multipath and noise was considered by correcting the tracked receiver clock offset.

2.5 | Other related work

Different from mitigating the multipath effects on the TOA estimation, another strategy is to exploit multipath signals for assisting positioning. Such an algorithm for LTE signals was provided in Ulmschneider and Gentner (2016) through estimating and tracking the parameters of all the arriving multipath components. An experimental site with a special scattering object was carefully chosen to demonstrate its effectiveness.

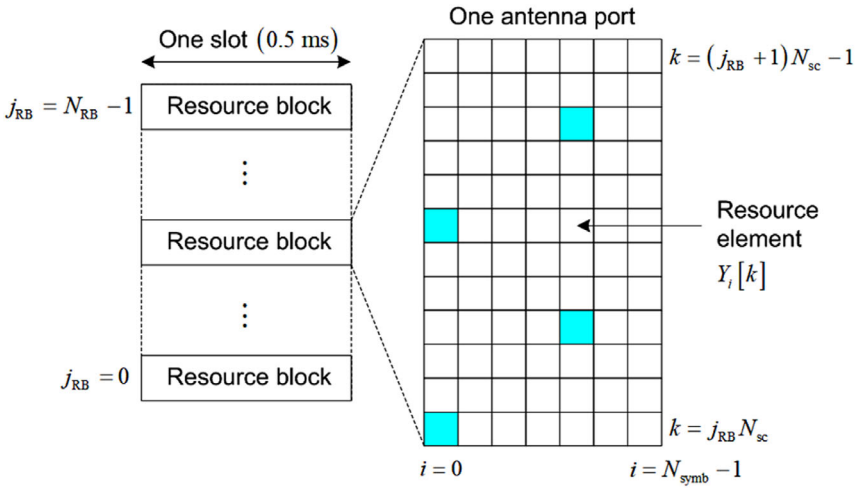

FIGURE 1 Time-frequency grid of an LTE signal for one slot and mapping of CRS pilot tones to resource elements [Color figure can be viewed in the online issue, which is available at wileyonlinelibrary.com and www.ion.org]

There are a number of TOA estimation algorithms for generic OFDM signals (Abrudan et al., 2013; Babich et al., 2017; Noschese et al., 2017, 2018; Wang et al., 2015; Yang et al., 2012) or other OFDM-based signals, e.g., WiFi signal (Lee et al., 2018), ultra-wideband (UWB) signal (Saberinia & Tewfik, 2008; Xu et al., 2008), and narrowband Internet-of-Things (NB-IoT) (Hu et al., 2019; Radnosrati et al., 2017). The channel estimation approaches for OFDM systems (Liu et al., 2014) also incorporate the TOA estimation required by the position determination. It is worth noting that these algorithms may also be applicable to LTE signal TOA estimation for positioning.

The above survey shows that a number of advanced TOA estimation algorithms for LTE signals aiming at counteracting multipath effects have been developed and evaluated by experiments with relatively mild multipath propagation conditions. Nevertheless, their performance assessment and comparison under complex multipath propagation conditions are not available in the literature. Hence, this paper aims to fill this gap.

3 | LTE FRAME STRUCTURE AND MULTIPATH PROPAGATION CHANNELS

LTE downlink data transmission is achieved based on OFDM modulation (3GPP, 2019a). With the assumption of a frequency division duplexing (FDD) scheme and normal cyclic prefix (CP), the downlink physical layer of the LTE system is organized by 10-ms radio frames. Each frame can be divided into 20 slots with a slot duration of 0.5 ms. Figure 1 shows the time-frequency grid of an LTE signal for one slot, composed of N_{RB} resource blocks (RBs). One RB includes $N_{\mathrm{sc}} = 12$ subcarriers and $N_{\mathrm{symb}} = 7$ symbols. The subcarrier index k and symbol index i are associated with a resource element (RE) $Y_i[k]$. The subcarrier spacing is $\Delta f = 15$ kHz, leading to a symbol interval $T_{\mathrm{symb}} = 66.67\ \mu$s.

Among various signals transmitted in the downlink physical layer, this paper focuses on exploiting the CRS for TOA estimation. Figure 1 also highlights the mapping of CRS to the REs by cyan grids. It is transmitted in symbol $i \in \{0, 4\}$ with the subcarrier spacing between two adjacent CRS pilot tones of $\Delta_{\mathrm{CRS}} = 6$.

During OFDM transmission, the total $N_r = N_{\mathrm{RB}}\ N_{\mathrm{sc}}$ frequency-domain samples for each symbol are first zero-padded to N_c to form a guard band. Next, an inverse discrete Fourier transform (IDFT) operator is adopted to obtain the time-domain discrete signal. This is then followed by adding CP at the beginning of each symbol. Finally, the digital-to-analog conversion and carrier modulation are performed to generate the transmitted radio-frequency signal.

For a multipath propagation channel, the CIR can be modeled as (Driusso et al., 2017)

$$h\ [n] = \sum_{l=0}^{L-1} \alpha_l \delta\left(n - \Delta\tau_l\right), \tag{1}$$

where L is the channel length; $\{\alpha_l\}$ denote the complex-valued path amplitudes; and $\{\Delta\tau_l\}$ are the multipath delays relative to the first arriving path. Note that the multipath delay is normalized by the sampling interval. The corresponding CFR is a harmonic model expressed by

$$H\ [k] = \sum_{l=0}^{L-1} \alpha_l e^{-j\frac{2\pi}{N_c}k\Delta\tau_l}. \tag{2}$$

In this paper, we consider several TDL channel models mentioned in the LTE technical specification (3GPP, 2019b) for performance evaluation. They are EPA, EVA, and ETU models, representing channels with a small, medium, and large delay spread, respectively. These channel models correspond to mixed line-of-sight (LOS)/NLOS

TABLE 1 Typical multipath propagation channel models in LTE technical specification and related multipath parameters

Channel model	Channel length	Path delays [m]	Path averaged powers [dB]	Maximum Doppler frequency [Hz]	NLOS probability
EPA	7	0, 9, 21, 27, 33, 57, 123	0.0, −1.0, −2.0, −3.0, −8.0, −17.2, −20.8	5	26.0%
EVA	9	0, 9, 45, 93, 111, 213, 327, 519, 753	0.0, −1.5, −1.4, −3.6, −0.6, −9.1, −7.0, −12.0, −16.9	70	27.2%
ETU	9	0, 15, 36, 60, 69, 150, 480, 690, 1500	−1.0, −1.0, −1.0, 0.0, 0.0, 0.0, −3.0, −5.0, −7.0	300	56.1%

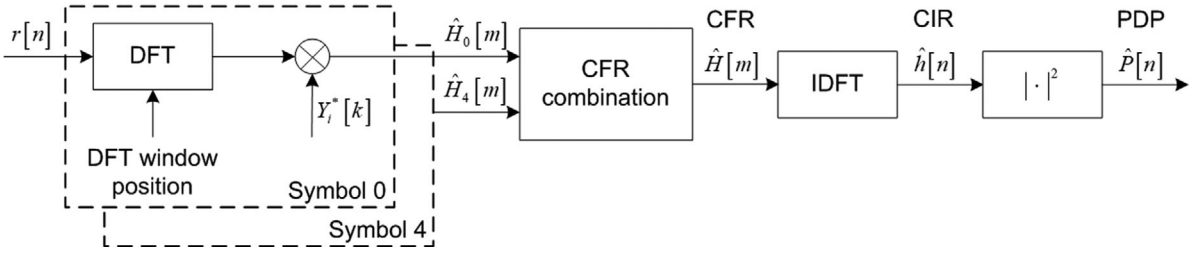

FIGURE 2 Block diagram of the channel estimation process

scenarios (del Peral-Rosado et al., 2018). To quantify the NLOS probability in each model, we implement 2,000 random channel realizations each for the 5-ms period and identify a channel realization as a NLOS case if the power of the first arriving path is at least 9 dB weaker than the total channel power over the 5-ms period (Del Peral-Rosado et al., 2016). Table 1 provides the specific multipath parameters of these models. Each model is characterized by a fixed number of channel paths with fixed relative delays and averaged powers. The amplitude of each path is a Rayleigh-distributed random variable with a Jakes Doppler spectrum (del Peral-Rosado et al., 2012c). The maximum Doppler frequencies used in the simulations are also given in Table 1 by considering the dynamic condition of each channel model. The EPA model has the lowest NLOS probability, and the ETU model has the highest NLOS probability. It has to be pointed out that the specific NLOS probability might vary with different LOS/NLOS identification approaches and threshold settings (Benedetto et al., 2007; Chen et al., 2014; Del Peral-Rosado et al., 2016).

4 | CHANNEL ESTIMATION

Channel estimation is essential for the OFDM system and can be achieved by exploiting the CFR measurements (Liu et al., 2014). The TOA estimation can then be easily extracted from the channel estimation results for the purpose of positioning. Figure 2 shows the block diagram of the channel estimation process in an LTE receiver (Shamaei & Kassas, 2018). We assume that the coarse symbol timing estimation is available, so it is feasible to remove the CP. The symbol timing error is assumed to be introduced by the physical channel and is equivalent to the TOA of the first arriving signal τ_0 (Yang et al., 2000). In the following, unless otherwise specified, the TOA is related to the first arriving signal. The receiver can thus transform the remaining N_c received samples $r[n]$ for the ith symbol into the frequency domain by a discrete Fourier transform (DFT). The CFR $\hat{H}_i[m], 0 \le m \le M-1$ can be obtained by multiplying the DFT output and the conjugate transmitted signal $Y_i^*[k]$ at the subcarriers allocated to the CRS. $M = N_r/\Delta_{\mathrm{CRS}}$ is the total number of CRS pilot tones for each symbol. To improve the estimation performance, the two CFR sequences, $\hat{H}_0[m]$ and $\hat{H}_4[m]$, obtained using the CRS transmitted in symbols $i = 0$ and 4 are merged into a $2M$-length CFR as (Driusso et al., 2017)

$$\hat{\mathbf{H}} = \begin{cases} \left[\hat{H}_0[0], \hat{H}_4[0], \ldots, \hat{H}_0[M-1], \hat{H}_4[M-1]\right]^T & \vartheta_0 < \vartheta_4 \\ \left[\hat{H}_4[0], \hat{H}_0[0], \ldots, \hat{H}_4[M-1], \hat{H}_0[M-1]\right]^T & \vartheta_0 > \vartheta_4 \end{cases}, \tag{3}$$

where $\vartheta_i \in \{0, \ldots, 5\}$ denotes the frequency-domain shift of the CRS transmitted in the ith symbol, satisfying $|\vartheta_0 - \vartheta_4| = 3$.

After this time-frequency combination, the CFR estimation for each slot can be written as (Wang & Morton, 2020)

$$\hat{H}[m] = \sum_{l=0}^{L-1} \alpha_l e^{-j\frac{2\pi}{N_c}\bar{m}\tau_l} + W[m], \tag{4}$$

where $\{\tau_l\} = \tau_0 + \{\Delta\tau_l\}$ are the TOAs of all the received signal components and $W[m]$ is the noise term. According to the subcarrier allocation specified in the LTE system (3GPP 2019a), the parameter $\bar{m}$ can be expressed by

$$\bar{m} = \begin{cases} m\Delta_{\mathrm{CRS}}/2 + \vartheta - N_r/2 & 0 \le m \le M-1 \\ m\Delta_{\mathrm{CRS}}/2 + \vartheta - N_r/2 + 1 & M \le m \le 2M-1 \end{cases}, \quad (5)$$

where $\vartheta = \min\{\vartheta_0, \vartheta_4\} \in \{0, 1, 2\}$.

The CIR can be obtained by applying an IDFT operator to the CFR as (Wang & Morton, 2020)

$$\begin{aligned} \hat{h}[n] &= \mathrm{IDFT}\left\{\hat{H}[m]\right\} \\ &\approx \frac{1}{2M}\sum_{l=0}^{L-1} \alpha_l e^{-j\frac{2\pi}{N_r}\left(\vartheta - \frac{N_r}{2}\right)\tau_l'} \sum_{m=0}^{2M-1} e^{j\frac{2\pi}{2M}m\left(n-\tau_l'\right)} \\ &\quad + w[n] \end{aligned} \quad (6)$$

for $n = 0, \ldots, 2M-1$, where $\tau_l' = \tau_l\ N_r/N_c$ and $w[n]$ is the time-domain noise term. The approximation in Equation (6) assumes that $e^{-j2\pi\tau_l/N_c} \approx 1$ by considering $\tau_l \ll N_c$. Then, the modulus square of the CIR, known as the PDP $\hat{P}[n]$, is computed.

Theoretically, under multipath propagation conditions, there exists multiple peaks in the CIR with time indices $\{n_l\} = \{\tau_l\}\ N_r/N_c$. This statement ideally assumes that all the multipath components are resolvable in the delay domain and their TOAs can be exactly converted to integer time indices. If the conventional CIR peak detection method is applied, the TOA estimation may easily deviate from its true value due to either a noise contribution or other delayed signals with stronger powers. This motivates the development of advanced TOA estimators capable of enhancing TOA estimation accuracy in complex multipath propagation channels discussed below.

5 | ADVANCED TOA ESTIMATION TECHNIQUES

In this section, we introduce several advanced TOA estimators with respect to their basic procedures and performance evaluation results. These methods may exploit one of the aforementioned channel estimation results. To increase the robustness in the presence of thermal noise, the channel estimation results within N_{slot} slots can be integrated as

$$\hat{C}\ [m] = \sum_{n_{\mathrm{slot}}=0}^{N_{\mathrm{slot}}-1} \hat{C}^{n_{\mathrm{slot}}}[m], \quad (7)$$

where $\hat{C}^{n_{\mathrm{slot}}}[m]$ can be the CFR, CIR, or PDP estimation for the n_{slot}th slot. In the simulations, the TOA value for the first arriving path τ_0 is fixed at 285 m to avoid intersymbol interference. This TOA value is randomly chosen without loss of generality. For each propagation channel model listed in Table 1, 2,000 channel realizations are conducted to obtain the statistical performance. The performance analysis for these techniques is also carried out for a simulated SNR range of −15 to 5 dB and the number of RBs N_{RB} at 25, 50, and 100. All the methods use an integration time of 10 slots, i.e., 5 ms. It should be clarified that the effect of an extended integration time on the TOA estimation accuracy is equivalent to an increased SNR value and thus will not be discussed in the following. The design parameter values used for performance evaluation are determined by extensive simulations for the FPD technique and according to what were used in the relevant literature for the SRA and DLL. For more details on the parameter selection process for the FPD technique, the interested reader can refer to the Appendix. In addition, the TOA estimation error is in units of meters.

5.1 | First peak detection technique

A simple, yet efficient method, which compares the PDP to a predefined threshold, is referred to as the FPD technique. The index of the first threshold-exceeding PDP sample is chosen as $\hat{n}_{\mathrm{TOA}}$. The TOA estimation can then be computed as $\hat{\tau}_0 = \hat{n}_{\mathrm{TOA}}\ N_c/N_r$. This technique is susceptible to the threshold settings. Thus, two specific threshold criteria are considered here for evaluating the TOA estimation performance.

5.1.1 | Threshold Criterion 1

Threshold criterion 1 is based on a normalized adaptive threshold as (Guvenc & Sahinoglu, 2005)

$$T_1 = T_{\mathrm{norm}}\ \left(\max\left\{\hat{P}[n]\right\} - \min\left\{\hat{P}[n]\right\}\right) + \min\left\{\hat{P}[n]\right\}, \quad (8)$$

where T_{norm} is the normalized threshold. $\max\{\cdot\}$ and $\min\{\cdot\}$ denote the maximum and minimum operators, respectively. Due to the involvement of the maximum value of $\hat{P}[n]$, the threshold T_1 is tightly related to the channel properties.

Figure 3 shows the cumulative distribution function (CDF) of the TOA estimation errors provided by the FPD technique based on threshold criterion 1 for different channel models and SNR values when $N_{\mathrm{RB}} = 100$. The errors with absolute values higher than 200 m are truncated to 200 m for a clearer display. There, $T_{\mathrm{norm}} = 0.4$ is assumed.

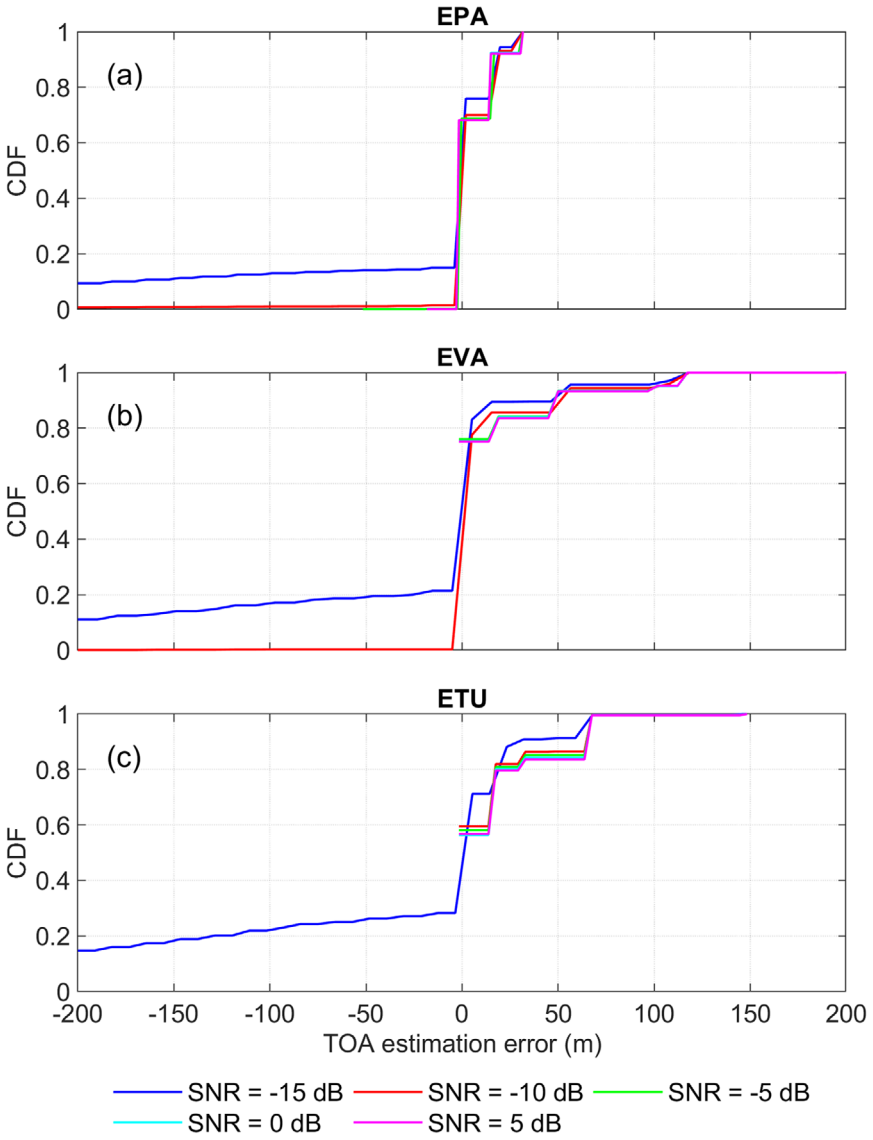

FIGURE 3 CDF of the TOA estimation errors provided by the FPD technique based on threshold criterion 1 for different channel models and SNR values when $N_{RB} = 100$ [Color figure can be viewed in the online issue, which is available at wileyonlinelibrary.com and www.ion.org]

TABLE 2 RMS of the TOA estimation errors (m) provided by the FPD technique based on threshold criterion 1 for different channel models and SNR values when $N_{RB} = 100$. The numbers in the bracket (··) indicate the RMS for LOS and NLOS scenarios

SNR (dB)	EPA	EVA	ETU
−15	83.76 (77.99 | 98.38)	95.70 (93.58 | 101.16)	108.52 (109.81 | 107.50)
−10	24.93 (22.72 | 30.38)	32.21 (22.26 | 49.90)	27.22 (16.59 | 33.25)
−5	11.52 (9.01 | 16.74)	32.95 (20.83 | 53.20)	28.29 (16.49 | 34.85)
0	11.50 (8.92 | 16.82)	33.16 (20.27 | 54.25)	28.99 (17.80 | 35.37)
5	11.62 (9.11 | 16.84)	33.34 (20.86 | 54.05)	29.55 (18.29 | 36.00)

Table 2 lists the root mean square (RMS) values of the TOA estimation errors for all the simulation conditions. Under each condition, we further separated LOS and NLOS scenarios. The RMS values for the two scenarios are listed next to the combined RMS values in the bracket (··). This same format of presenting the RMS values for overall and separate LOS and NLOS scenarios will be used in the following tables and figures.

As can be observed from Figure 3 and Table 2, the estimation accuracy degrades obviously for SNR = −15 dB. This is due to a high probability of early estimations in the presence of high noise. For SNR values higher than −10 dB, the technique yields a nearly constant accuracy level. The high positive TOA estimation errors are due to the channel NLOS conditions, i.e., the first arriving signal experiences a much deeper fading compared to other later arriving

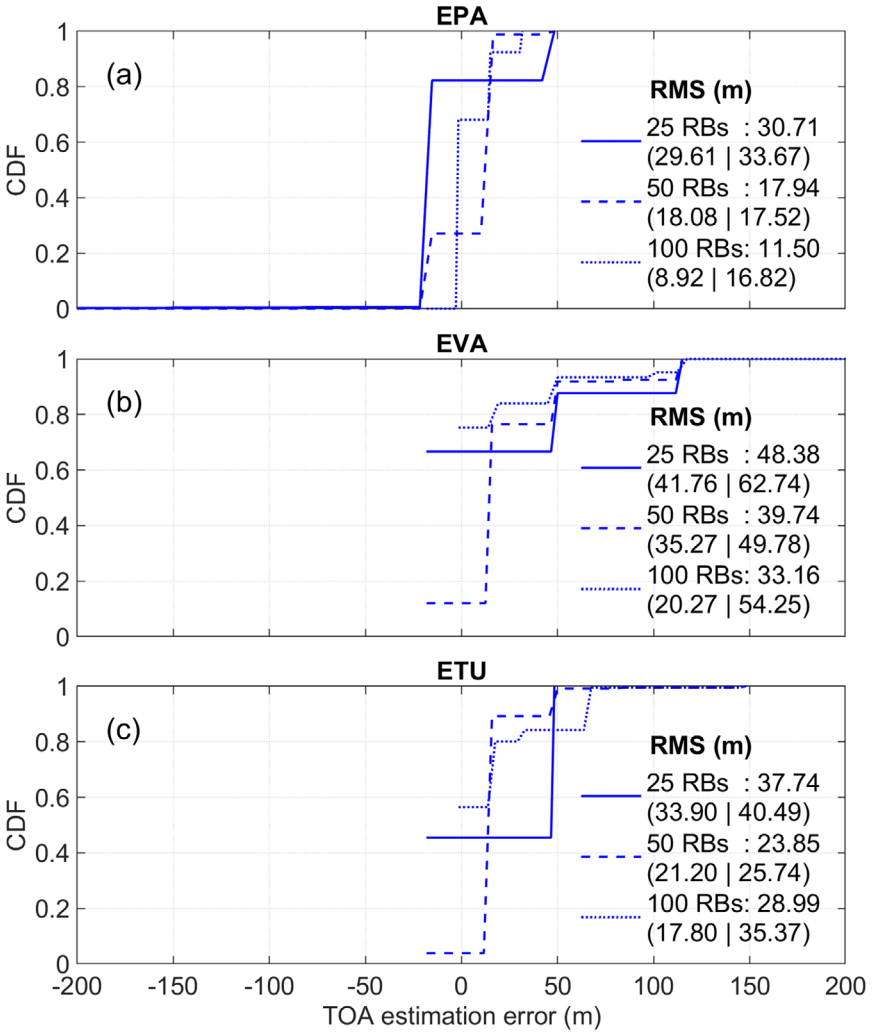

FIGURE 4 CDF and RMS of the TOA estimation errors provided by the FPD technique based on threshold criterion 1 for different channel models and numbers of RBs when SNR = 0 dB [Color figure can be viewed in the online issue, which is available at wileyonlinelibrary.com and www.ion.org]

signals. Under each condition, the estimation accuracy in NLOS scenarios is degraded compared to LOS scenarios. The technique can be improved to better mitigate the noise effects by using a larger normalized threshold. It should be pointed out that if the normalized threshold is too large, it would cause late estimations for the NLOS cases. The step-shape cumulative probability shown in Figure 3 is caused by the discrete TOA estimations.

Figure 4 displays the effect of N_{RB} (equivalent to signal bandwidth) on estimation performance of the FPD technique based on threshold criterion 1, considering three channel models and a fixed SNR of 0 dB. The RMS value of the overall TOA estimation errors and those for LOS and NLOS scenarios are also given in the legend of Figure 4. Understandably, a larger N_{RB} implies a smaller sampling period and an improved multipath resolution capability. Therefore, for most scenarios, a higher signal bandwidth is beneficial for improving the estimation accuracy. One exceptional case is that for the ETU model, where the RMS is slightly larger when increasing N_{RB} from 50 to 100. This is because the strong later arriving paths in the ETU model become distinguishable for $N_{\mathrm{RB}} = 100$. One of the later arriving paths may be mistaken as the first arriving path when the real first arriving path experiences a deep fading, leading to large estimation errors.

5.1.2 | Threshold Criterion 2

Another criterion to determine a threshold is based on a fixed early detection probability. As the noise-only bin in PDP follows a central χ^2 distribution with $\nu = 2N_{\mathrm{slot}}$ degrees-of-freedom (DOF), the early detection probability can be modeled as (Dardari et al., 2008)

$$P_{\mathrm{ed}} = 1 + \frac{(1 - q_{\mathrm{noise}})^{N_{\mathrm{TOA}}} - 1}{N_{\mathrm{TOA}} q_{\mathrm{noise}}}, \tag{9}$$

where N_{TOA} is the number of possible TOA values, which should be set empirically for practical implementation. q_{noise} is the probability of a noise-only PDP sample above a threshold T_2 and can be computed as (Giorgetti & Chiani,

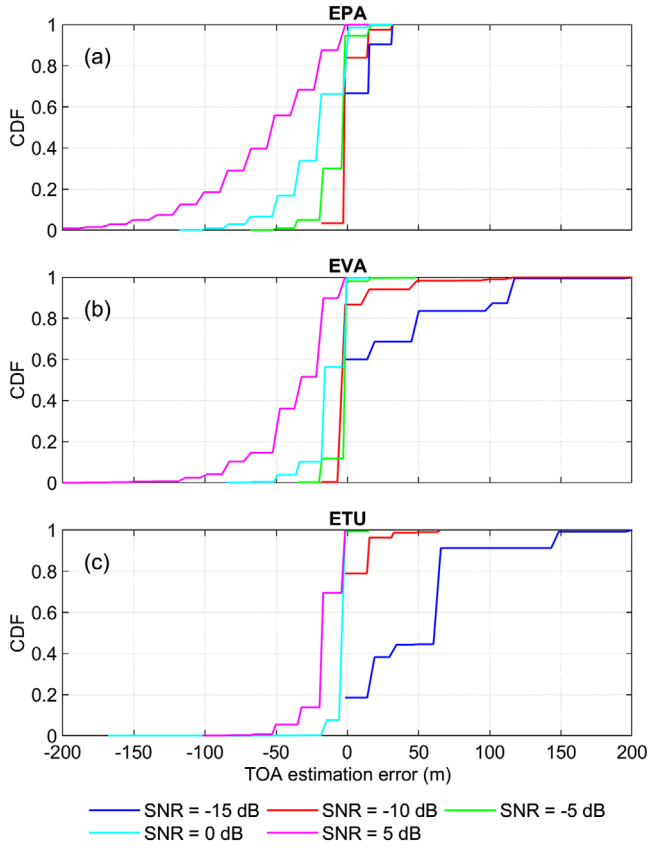

FIGURE 5 CDF of the TOA estimation errors provided by the FPD technique based on threshold criterion 2 for different channel models and SNR values when $\boldsymbol{N_{RB}} = 100$ [Color figure can be viewed in the online issue, which is available at wileyonlinelibrary.com and www.ion.org]

2013; Torrieri, 2005)

$$q_{\text{noise}} = \exp\left(-\frac{T_2}{2\sigma^2}\right)\sum_{q=0}^{\nu/2-1}\frac{1}{q!}\left(\frac{T_2}{2\sigma^2}\right)^q, \qquad (10)$$

where σ^2 is the noise variance for the real or imaginary part of the noise component $w[n]$ in the CIR estimation for each slot. Therefore, the threshold T_2 can be determined in terms of a preset P_{ed} according to Equations (9) and (10).

The CDF of the TOA estimation errors obtained with the FPD technique based on threshold criterion 2 for different channel models and SNR values when $N_{\text{RB}} = 100$ is illustrated in Figure 5. The number of the TOA estimations and RMS values of the TOA estimation errors for all the simulation conditions are summarized in Table 3. P_{ed} is set to 10^{-6}, and N_{TOA} is computed based on a possible TOA range of 0 to 300 m. The noise variance in the PDP is also assumed to be available.

This threshold criterion does not involve the signal strength information and thus is not related to the channel properties. In case of low SNR conditions, no threshold-crossing may occur. This enhances the capability of noise resistance, but yields less measurements. As can be seen from Table 3, the RMS of the TOA estimation errors first decreases when increasing the SNR as the number of high positive estimation errors is reduced. However, if the SNR further increases, the RMS increases instead. This can be explained by the fact that the TOAs of the received signals may not correspond to discrete time indices in the CIR according to $\{n_l\} = \{\tau_l\}\, N_r/N_c$. The spectral leakage effect occurs in the IDFT operation for estimating the CIR, but is not taken into account in the threshold criterion 2. The leaked signal energy in the noise-only bins becomes stronger and thus causes more early estimation results for higher SNR signals as shown in Figure 5. Similarly, for the same SNR value (≥ -5 dB), the EPA model with stronger power distributed at the short-delay paths yields a higher probability of early estimation results and a larger RMS value in comparison with the other two models. From this point of view, a smaller early detection probability should be set to alleviate early estimations. Meanwhile, this would decrease the number of measurements in low SNR conditions or yield wrong estimation results for channel realizations with strong, later arriving signals.

Figure 6 shows the CDF and RMS of the TOA estimation errors provided by the FPD technique based on threshold criterion 2 for different channel models and numbers of RBs when SNR = 0 dB. It can be clearly seen that a larger number of RBs enhances the estimation accuracy due to the higher timing resolution. Moreover, as the technique

TABLE 3 Number of the TOA estimations and RMS of the TOA estimation errors (m) provided by the FPD technique based on threshold criterion 2 for different channel models and SNR values when $N_{\text{RB}} = 100$. The numbers in the bracket (··) indicate the RMS for LOS and NLOS scenarios

	EPA		EVA		ETU	
SNR (dB)	#	RMS (m)	#	RMS (m)	#	RMS (m)
−15	1720	12.30 (9.79 | 18.02)	1620	53.77 (43.18 | 76.43)	1518	75.18 (67.30 | 80.68)
−10	1978	8.29 (6.23 | 12.44)	2000	19.47 (11.34 | 32.40)	2000	10.66 (2.97 | 13.99)
−5	2000	13.32 (12.55 | 15.31)	2000	7.37 (7.14 | 7.95)	2000	2.00 (1.67 | 2.23)
0	2000	31.78 (30.20 | 35.92)	2000	18.73 (19.11 | 17.66)	2000	6.67 (8.86 | 4.23)
5	2000	72.29 (68.43 | 82.29)	2000	46.34 (46.45 | 46.05)	2000	21.41 (22.59 | 20.45)

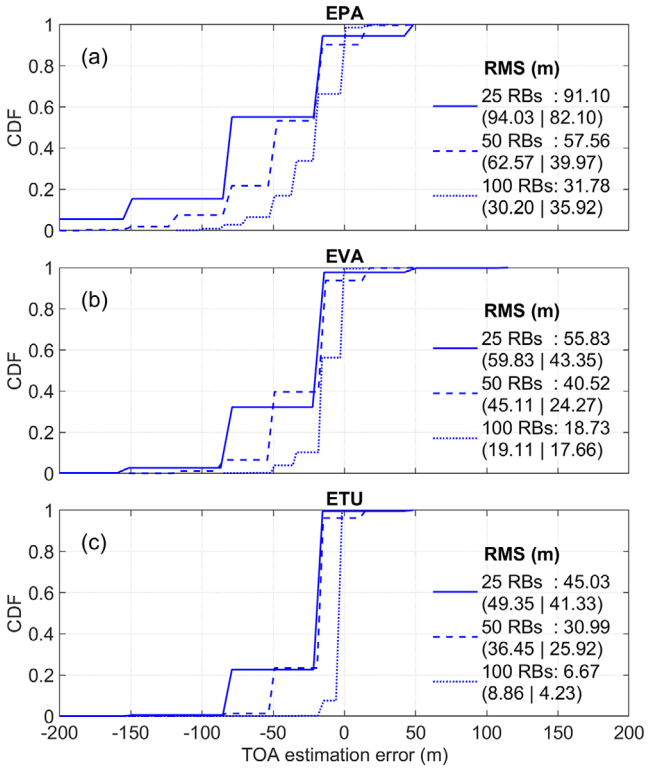

FIGURE 6 CDF and RMS of the TOA estimation errors provided by the FPD technique based on threshold criterion 2 for different channel models and numbers of RBs when SNR = 0 dB [Color figure can be viewed in the online issue, which is available at wileyonlinelibrary.com and www.ion.org]

is susceptible to the spectral leakage effect, the LOS cases with a stronger first arriving path lead to a higher RMS value relative to the NLOS cases.

5.2 | Information theoretic criteria technique

The ITC technique was initially intended to provide a TOA estimation for UWB signals based on the statistical properties of the energy detector outputs (Giorgetti & Chiani, 2013). It is also applicable to LTE signals by using the underlying statistical characteristics of the PDP.

Unlike the integration operation in Equation (7) for other techniques, the PDP estimations over N_{slot} slots are arranged in a N_{slot}-by-$2M$ matrix $\mathbf{P}$ for the ITC method. Theoretically, the noise-only bin in $\mathbf{P}$ follows a central χ^2 distribution, whereas the signal-plus-noise bin follows a non-central χ^2 distribution with a non-centrality parameter depending on the path gain. There are two implementation schemes for this technique in Giorgetti and Chiani (2013). Here, we only elaborate the ITC technique based on early bins for the reader's convenience. The three main steps of the ITC technique are illustrated as follows:

1. Build the averaged PDP vector $\bar{\mathbf{p}}$ by computing the mean of each column in $\mathbf{P}$ and find the index $m_{\max}$ of the maximum in $\bar{\mathbf{p}}$. The first $m_{\max}+1$ columns in $\mathbf{P}$ and $\bar{\mathbf{p}}$ are regarded as $\mathbf{P}_E$ and $\bar{\mathbf{p}}_E$, respectively.
2. The cost function values for all the possible model orders $k = 1, \dots, m_{\max}$ are computed. For the kth model, the first k columns in $\mathbf{P}_E$ correspond to noise-only bins, while the remaining columns correspond to signal-plus-noise bins. $\bar{\mathbf{p}}_E$ contains the information to calculate the distribution parameters for each bin in $\mathbf{P}_E$. The log-likelihood of each element in $\mathbf{P}_E$ is then evaluated. The cost function is computed using all the log-likelihood values and the penalty function associated with the kth model.
3. The TOA estimation is $\hat{\tau}_0 = \hat{k}\ N_c/N_r$, where $\hat{k}$ is the model order which minimizes the cost function.

Note that the detailed equations used in the above steps can be found in Giorgetti and Chiani (2013). As suggested in Driusso et al. (2017), a windowing operation is applied to the PDP to reduce the biasing effect of sidelobes. The central chi-square approximation is used in computing the log-likelihood, and the efficient detection criteria is used for the penalty function. The CDF and statistical results of the TOA estimation errors obtained with the ITC algorithm for different channel models and SNR values when $N_{\text{RB}} = 100$ are given in Figure 7 and Table 4, respectively.

Figure 7 indicates that the technique generates early estimation results in most of the channel realizations for SNR higher than −10 dB. This is caused by the high sensitivity to the spectral leakage effect occurring in the CIR. Because of this, the RMS value for LOS cases in the EVA/ETU channel is even higher than that for NLOS cases as shown in Table 4. Nevertheless, when SNR = −15 dB, the technique provides poor estimation accuracy owing to the large positive estimation errors. This is because the detected PDP bin with maximum energy is far from that of the first arriving signal in the presence of high noise. Some noise-only bins exist between the bins containing the first arriving signal and with maximum energy, failing to comply with the PDP bin classification in Step 2 of the ITC algorithm. Thus, as can be observed from Table 4, the estimation accuracy first becomes better when increasing the SNR, but then becomes worse with further increase of the SNR. Overall, this technique is robust to the harsh multipath conditions for medium SNR values.

Figure 8 shows the estimation performance provided by the ITC method for different N_{RB} values and three channel models when SNR = 0 dB. Since the ITC approach generates discrete TOA estimations like the FPD technique does, it provides an improved estimation accuracy if a higher N_{RB} is used in the LTE system.

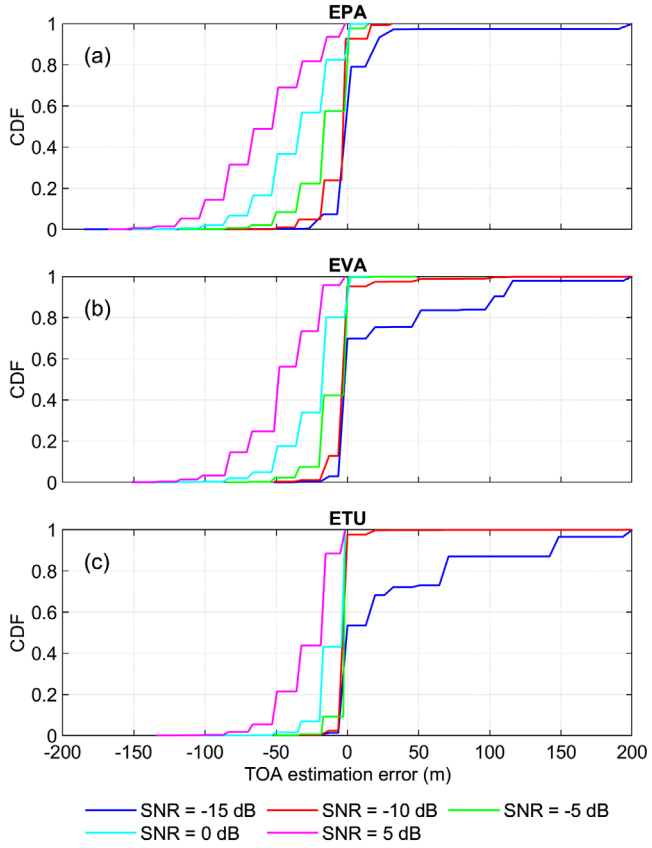

FIGURE 7 CDF of the TOA estimation errors provided by the ITC algorithm for different channel models and SNR values when $N_{RB} = 100$ [Color figure can be viewed in the online issue, which is available at wileyonlinelibrary.com and www.ion.org]

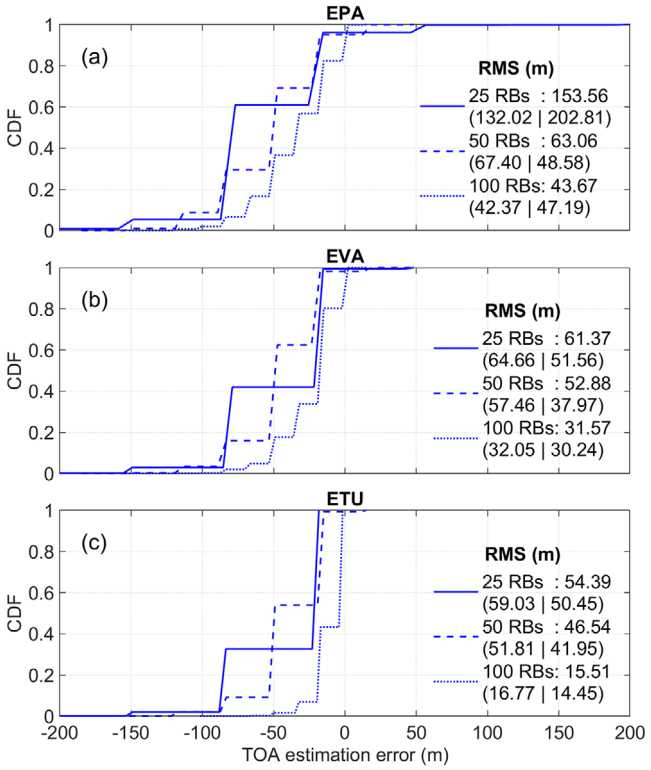

FIGURE 8 CDF and RMS of the TOA estimation errors provided by the ITC method for different channel models and numbers of RBs when SNR = 0 dB [Color figure can be viewed in the online issue, which is available at wileyonlinelibrary.com and www.ion.org]

5.3 | Super-resolution algorithm

Because the CFR for a multipath propagation channel in Equation (2) is a harmonic signal model, the TOA estimation problem is equivalent to the spectral estimation problem by exchanging the time and frequency variables. Based on this, the application of an SRA to frequency-domain channel measurements was investigated for TOA estimation in Li and Pahlavan (2004).

Here, we adopt the ESPRIT as a representative of SRAs for illustration. This algorithm has been well documented in Driusso et al. (2017) and Shamaei and Kassas (2018). We only summarize the key steps as follows:

1. Construct a P-by-$(2M - P + 1)$ frequency-domain data matrix using the CFR and perform singular value decomposition (SVD) of the data matrix.
2. Estimate the channel length by the minimum description length (MDL) criterion using the singular values obtained in Step 1.
3. Construct the ESPRIT rotational matrix and compute its eigenvalues.
4. Compute the delay estimations for all the detected paths using the phase information in the eigenvalues obtained in Step 3. The smallest delay estimation is considered as $\hat{\tau}_0$.

TABLE 4 RMS of the TOA estimation errors (m) provided by the ITC algorithm for different channel models and SNR values when $N_{RB} = 100$. The numbers in the bracket (··) indicate the RMS for LOS and NLOS scenarios

SNR (dB)	EPA	EVA	ETU
−15	573.58 (474.85 | 790.17)	417.79 (383.32 | 498.46)	270.61 (191.42 | 319.25)
−10	12.75 (12.37 | 13.78)	17.88 (13.15 | 26.70)	19.58 (4.16 | 25.89)
−5	24.22 (23.24 | 26.82)	15.88 (15.99 | 15.58)	6.37 (7.29 | 5.55)
0	43.67 (42.37 | 47.19)	31.57 (32.05 | 30.24)	15.51 (16.77 | 14.45)
5	67.57 (66.08 | 71.65)	53.18 (53.32 | 52.82)	34.20 (35.40 | 33.23)

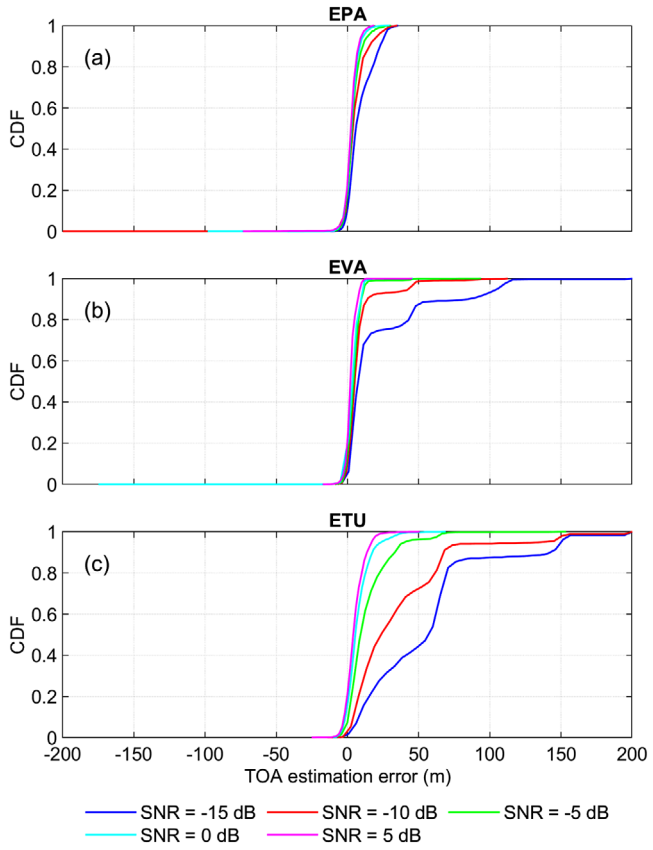

FIGURE 9 CDF of the TOA estimation errors provided by the SRA for different channel models and SNR values when $\boldsymbol{N_{RB}} = 100$ [Color figure can be viewed in the online issue, which is available at wileyonlinelibrary.com and www.ion.org]

According to Yang et al. (2000), we can reasonably adjust the true TOA to be a positive value after coarse symbol synchronization during the TOA estimation. Owing to this intrinsic constraint, the results with negative $\hat{\tau}_0$ are discarded. Figure 9 illustrates the CDF of the TOA estimation errors using the SRA for different channel models and SNR values when $N_{RB} = 100$. The number of the TOA estimations and RMS values of the TOA estimation errors for all the simulation conditions are given in Table 5. The design parameter P is assumed to be M (Driusso et al., 2017; Shamaei & Kassas, 2018).

The algorithm's performance is tightly related to the channel length estimation, which is in turn dependent on the SNR condition. As mentioned in Driusso (2016), Liavas et al. (1999), and Via et al. (2006), our simulations also indicate that the MDL criterion tends to underestimate or overestimate the channel length for relatively low or high SNR values, resulting in a large number of invalid negative TOA estimations. Accordingly, the number of estimations is sharply reduced, especially for the ETU channel with SNR = −15 or 5 dB. Moreover, the RMS of the TOA estimation errors increases with the decreasing SNR. Contrary to other techniques, the TOA estimations obtained with the SRA are not confined to discrete values. Overall, the SRA performs well in a wide range of SNR conditions and several channel types due to its promising time-domain resolution of the channel response. This algorithm, however, also has a high computational cost, making it impractical for real-time implementation.

Figure 10 shows the statistical results of the TOA estimation errors using the SRA in case of three N_{RB} values for three channel models and a fixed SNR of 0 dB. The CDF curves and RMS values demonstrate the improvement in the estimation accuracy with a larger N_{RB} value and the better accuracy in LOS scenarios.

5.4 | Delay-lock loop

The DLL with a block diagram shown in Figure 11 takes advantage of a closed-loop architecture to estimate the TOA. With consideration of the OFDM modulation in the LTE signal, the correlation process is performed in the frequency domain. At the beginning of each loop updating period, the integer and fractional parts of the TOA estimation $\hat{\tau}_0$ are used to control the DFT window position and perform phase rotation, respectively. Next, the correlation results in early and late branches are obtained by shifting the CRS sequence with ξ and $-\xi$ samples, respectively. Then, a discriminator exploits the early and late correlation results to calculate the residual in the TOA estimation. Finally, the filtered residual is used to adjust the TOA estimation for the next updating period. The TOA can be

TABLE 5 Number of the TOA estimations and RMS of the TOA estimation errors (m) provided by the SRA for different channel models and SNR values when N_{RB}= 100. The numbers in the bracket (··) indicate the RMS for LOS and NLOS scenarios

	EPA		EVA		ETU	
SNR (dB)	#	RMS (m)	#	RMS (m)	#	RMS (m)
−15	1934	12.46 (10.21 | 17.38)	1926	41.64 (36.01 | 54.03)	757	124.09 (155.35 | 89.69)
−10	1992	9.95 (8.25 | 13.67)	1993	15.73 (11.49 | 23.58)	1882	79.59 (69.51 | 86.74)
−5	1993	6.71 (4.31 | 11.00)	1992	7.53 (5.10 | 11.79)	1989	20.59 (18.24 | 22.26)
0	1990	5.84 (4.30 | 8.86)	1946	6.62 (6.01 | 8.03)	1940	11.26 (9.90 | 12.22)
5	1993	5.64 (4.56 | 7.96)	1485	4.30 (2.85 | 6.77)	1325	8.22 (6.91 | 9.11)

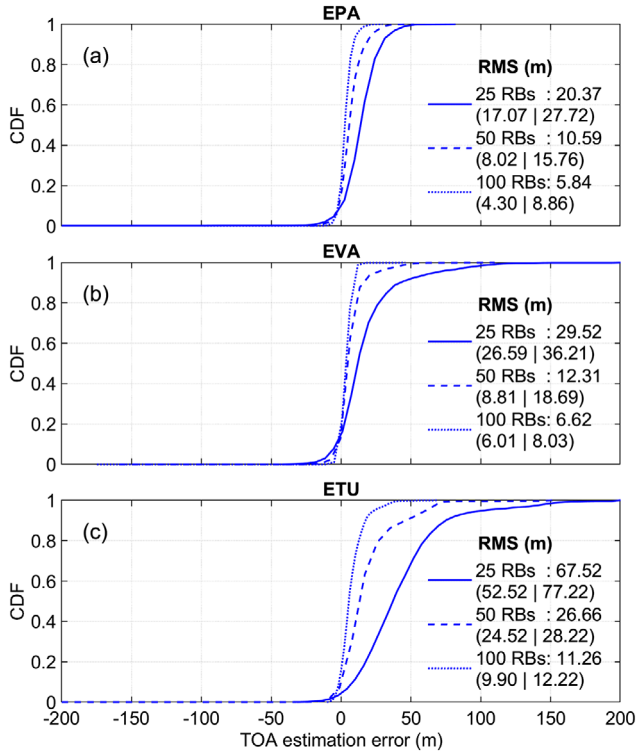

FIGURE 10 CDF and RMS of the TOA estimation errors provided by the SRA for different channel models and numbers of RBs when SNR = 0 dB [Color figure can be viewed in the online issue, which is available at wileyonlinelibrary.com and www.ion.org]

tracked in a locked status when the energies in early and late branches are close to each other.

The main weakness of the DLL for tracking LTE signals is its narrow pull-in range in the delay domain (Shamaei & Kassas, 2018; Yang et al., 2000). This implies that an accurate TOA estimation must be provided by other techniques for initializing the DLL. However, as shown by the previous simulation results, there is still a high probability of large TOA estimation errors in complex multipath propagation channels. If an inaccurate initial estimation is used, the DLL may track one of the later arriving signals instead and yield an unacceptable estimation error.

In the multipath propagation channel, the multipath effect is the dominant factor of the tracking error in the DLL (Yang et al., 2000). Following the common metric for analyzing the multipath mitigation performance of a closed-loop architecture (Townsend et al., 1995), Figure 12 presents the multipath error envelope provided by the DLL for different N_{RB} values. A two-path model with a fixed multipath to direct signal power ratio (MDR) of −1 dB is used, and a noise-free environment is assumed in the simulations. The correlator spacing ξ is set to 0.5 samples (Shamaei & Kassas, 2018; Yang et al., 2000). The two curves for each N_{RB} value correspond to in-phase and out-of-phase multipath cases. As can be seen, the DLL suffers from a TOA tracking bias, depending on the multipath parameters and signal bandwidth. A higher signal bandwidth brings a considerable reduction in the TOA tracking bias.

6 | COMPARISON AND DISCUSSION

This section first provides comparisons in terms of accuracy and complexity among these advanced algorithms and then discusses the key characteristics of each algorithm in detail.

6.1 | Accuracy comparison

To allow an intuitive comparison, Figure 13 compares the RMS values of the TOA estimation errors as a function of SNR for different channel models obtained with the aforementioned advanced algorithms except for the DLL when $N_{\mathrm{RB}} = 100$. It demonstrates that in cases of medium SNR values, all the advanced algorithms provide comparable TOA estimation accuracy in these multipath propagation channels.

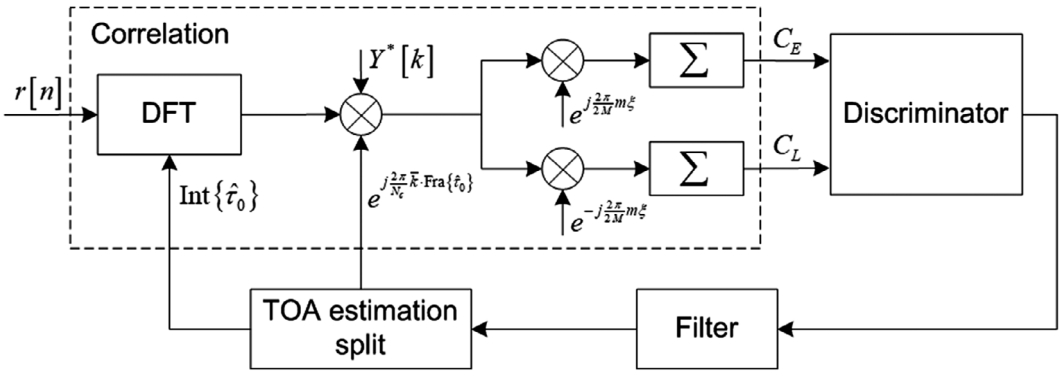

FIGURE 11 Block diagram of the DLL for tracking the LTE signal TOA

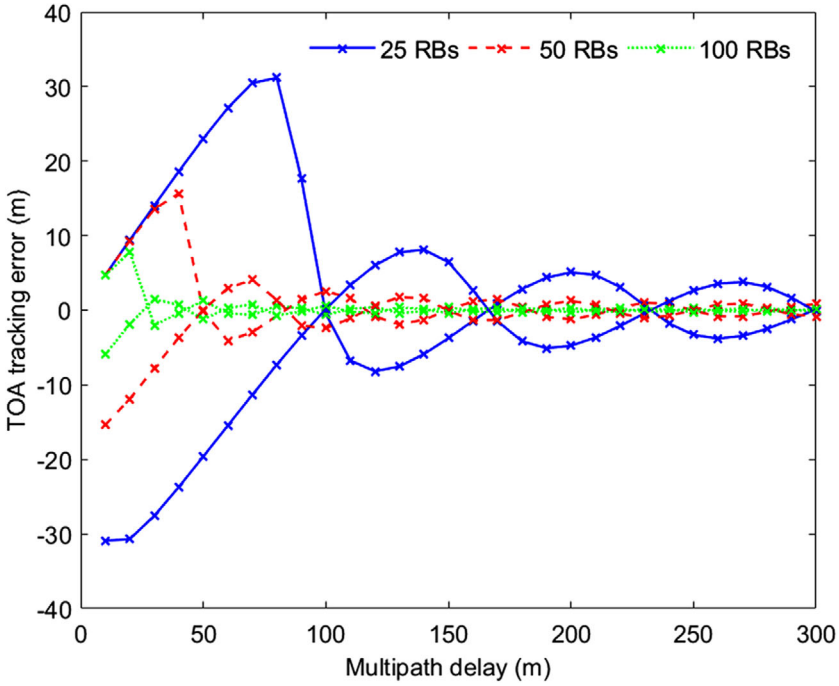

FIGURE 12 Multipath error envelope provided by the DLL for different numbers of RBs and a fixed MDR of −1 dB [Color figure can be viewed in the online issue, which is available at wileyonlinelibrary.com and www.ion.org]

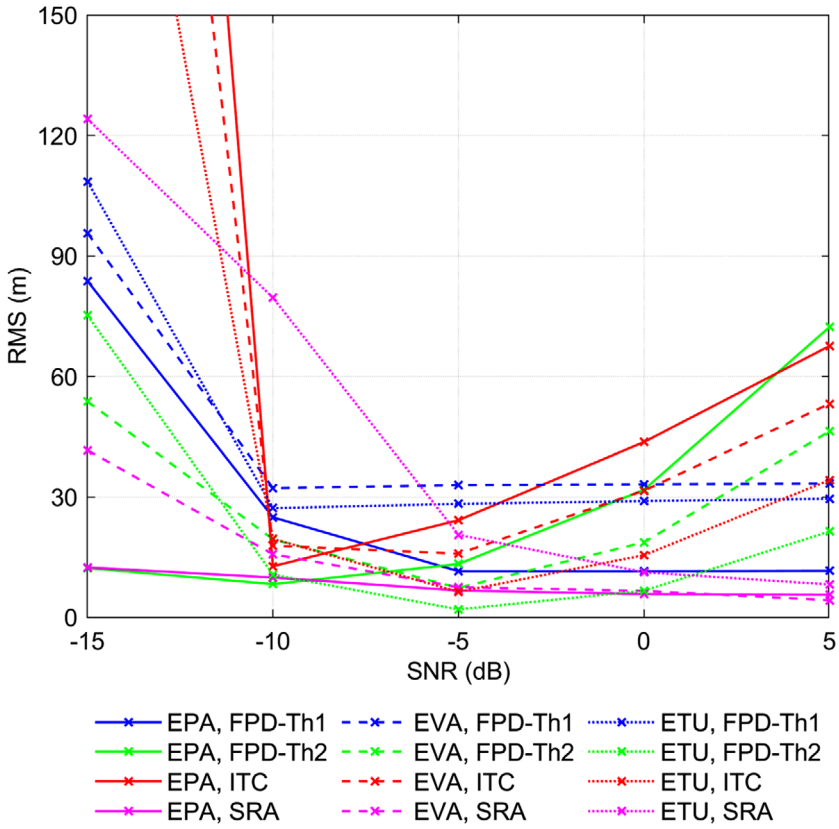

FIGURE 13 RMS of the TOA estimation errors versus SNR for different channel models obtained with several advanced TOA estimators when $N_{RB} = 100$ [Color figure can be viewed in the online issue, which is available at wileyonlinelibrary.com and www.ion.org]

Nevertheless, in cases of relatively low and high SNR values, the performance differences among these methods are notable. If only the statistical accuracy is taken into account, Table 6 summarizes the preferred algorithms under different conditions. The FPD technique with threshold criterion 1 can be used for the EPA channel in a high SNR condition. The FPD technique based on threshold criterion 2 is preferred for low SNR values. The SRA is a promising method except for the ETU channel with a low SNR value.

TABLE 6 Preferred algorithms under different channel models and SNR conditions

Channel model	SNR	Preferred algorithms
EPA	Low	FPD-Th2, SRA
	High	FPD-Th1, SRA
EVA	Low	FPD-Th2, SRA
	High	SRA
ETU	Low	FPD-Th2
	High	SRA

6.2 | Complexity comparison

In this subsection, we analyze and compare the computational complexity associated to the number of multiplications involved in the aforementioned techniques. Since all techniques require the CFR estimation, we only examine the signal processing procedures after the CFR estimation for generating one TOA estimation in the following analysis.

The FPD and ITC techniques both exploit the PDP estimations over N_{slot} slots. For each slot, the IDFT operation for the CIR estimation requires $O(2M\log(2M))$ multiplications. The PDP estimation is then obtained by a modulus square operation with $O(2M)$ multiplications. The remaining procedures in the FPD technique incorporate a few times of peak finding in the integrated PDP. For the ITC, the PDF of central chi-square distributions for different distribution parameters can be stored in a look-up table. The evaluation of the log-likelihood for calculating the cost functions can thus be achieved by table look-up operations, leading to a significantly decreased complexity. The final step is to find the model order, which minimizes the cost function. The computational cost of these operations is negligible compared to the calculation of the PDP estimations. Therefore, the total numbers of multiplications required by the FPD and ITC approaches can both be approximated as $O([2M\log(2M) + 2M]N_{\text{slot}})$.

For the SRA, the most demanding procedures are those matrix operations. The SVD of the frequency-domain data matrix requires $O(P^2K)$ multiplications. Computing the MDL criterion requires many fewer multiplications than the SVD operation. The number of multiplications to calculate the ESPRIT rotational matrix is $O(P^2\hat{L} + 2(P-1)P\hat{L} + 2\hat{L}^3 + 2(P-1)\hat{L}^2)$. The eigenvalue decomposition of the ESPRIT rotational matrix requires $O(\hat{L}^3)$ multiplications. Therefore, the total number of multiplications used by the SRA can be expressed by $O(P^2(K+\hat{L}) + 2(P-1)(P+\hat{L})\hat{L} + 3\hat{L}^3)$. In our simulations, we have $P = M$, $K = M+1$, and $\hat{L} \ll M$. Thus, the number of multiplications can be approximated as $O(M^3 + 2M^2\hat{L})$.

The main computational complexity of the DLL comes from the correlation process. To compute an early and a late correlation result, the DLL consumes $O(4M)$ multiplications.

Therefore, the complexity of SRA is much higher than those of other techniques. The DLL is the most computationally efficient one. The complexities of the FPD and ITC algorithms are in the same order of magnitude if we ignore the large number of table loop-up operations required by the ITC algorithm.

6.3 | Discussion for each algorithm

The FPD method largely depends on the predefined threshold to achieve a desirable performance. Two threshold criteria are examined to assess its performance. Criterion 1 computes an adaptive threshold using the maximum and minimum values of the channel estimation result and a preset normalized threshold. This criterion leads to a number of early estimations and thus a poor TOA estimation accuracy for low SNR values. A high, normalized threshold would be beneficial to enhance noise resistance. However, late estimations may occur when using a high, normalized threshold for the propagation condition if the first arriving path is much more attenuated than other later arriving paths. Hence, the normalized threshold in this criterion should be chosen carefully based on the propagation channel and SNR condition.

Criterion 2 used for the FPD method determines the threshold according to a fixed early detection probability. The threshold is thus irrelevant to the channel properties. It should be noted that the spectral leakage effect in the CIR estimation introduces an increased number of early estimations in this technique for a higher SNR condition. Moreover, this technique eliminates the early estimations, but also reduces the number of measurements for a low SNR value. Therefore, both the measurement availability and estimation accuracy need to be considered for choosing a reasonable early detection probability.

The ITC technique is also highly sensitive to the spectral leakage occurring in the CIR estimation. The TOA estimation performance obtained with the ITC algorithm adversely deteriorates for increasing SNR values except for very low SNR values. The technique is robust to the harsh multipath condition for medium SNR values and does not require a parameter tuning for different conditions. Nevertheless, the performance would experience a drastic degradation if the SNR value is too low or too short an integration time is used.

The SRA has a superior multipath resolution capability at the cost of a high computational complexity. It incorporates a channel length estimation procedure based

on the MDL criterion. Either an underestimated channel length in a low SNR condition or an overestimated channel length in a high SNR condition would reduce the number of estimations. Additionally, this algorithm provides an improved TOA estimation accuracy for a higher SNR value.

The DLL method is different from the others owing to its closed-loop architecture. It requires an accurate TOA estimation provided by other techniques for initialization. An improper initial value would lead to the DLL's failure to track the LTE signal TOA. In addition, it still suffers from a notable tracking bias due to the multipath effects.

7 | SUMMARY

In this paper, we first reviewed the existing literature concerning the TOA-based positioning using LTE signals and the relevant positioning performance assessment. With the channel estimation results obtained in an LTE receiver, we illustrated the key steps in the FPD, ITC, SRA, and DLL techniques to generate the TOA estimation for LTE signals. Numerous computer simulations were conducted to evaluate their estimation performances for several realistic multipath propagation channels in the presence of AWGN. Simulation results indicate that all the advanced algorithms generate comparable and reasonable TOA estimation accuracy in these multipath propagation channels for medium SNR values. Nevertheless, they perform very differently for relatively low and high SNR values. All of the techniques can benefit from a higher LTE signal bandwidth to statistically reduce the TOA estimation error.

In addition to estimation accuracy, some other features of each technique should be noted. The FPD technique has a simple implementation, but relies on a careful choice of the threshold-related parameters. Moreover, the FPD technique based on threshold criterion 2 may lead to a decreased number of measurements under low SNR conditions. The ITC technique needs a relatively long integration time to guarantee reliable estimations. The SRA suffers from a high computational complexity due to the matrix operations and needs to discard some measurements if the channel length estimation is inaccurate. The DLL is suitable for low dynamic conditions and requires an accurate initial estimation from other techniques. In practical applications, the choice of a suitable TOA estimator for LTE signal depends on the receiver environment and user requirements.

We should point out that this work only investigated a specific heuristic strategy to discriminate dynamic LOS/NLOS channel conditions in each model for performance assessment. However, LOS and NLOS affect the TOA estimation differently. Hence, effectively identifying the channel between LOS and NLOS scenarios would be critical to improve the TOA estimation accuracy, e.g., by setting appropriate design parameters in the TOA estimators. The LOS/NLOS channel identification using real collected LTE data is under investigation and will be the subject of a subsequent publication.

ACKNOWLEDGEMENT

This work is funded by the University of Colorado, Boulder.

ORCID

Pai Wang https://orcid.org/0000-0002-9686-609X

REFERENCES

3GPP. (2010). *LTE, Evolved Universal Terrestrial Radio Access (E-UTRA); Physical channels and modulation* (3GPP TS 36.211 version 9.1.0 release 9). European Telecommunications Standards Institute.

3GPP. (2019a). *LTE, Evolved Universal Terrestrial Radio Access (E-UTRA); Physical channels and modulation* (3GPP TS 36.211 version 15.6.0 release 15). European Telecommunications Standards Institute.

3GPP. (2019b). *LTE, Evolved Universal Terrestrial Radio Access (E-UTRA); Base Station (BS) radio transmission and reception* (3GPP TS 36.104 version 16.1.0 release 16). European Telecommunications Standards Institute.

Abrudan, T. E., Haghparast, A., & Koivunen, V. (2013). Time synchronization and ranging in OFDM systems using time-reversal. *IEEE Transactions on Instrumentation and Measurement*, *62*(12), 3276–3290. https://doi.org/10.1109/TIM.2013.2272840

Babich, F., Noschese, M., Marshall, C., & Driusso, M. (2017, May). A simple method for ToA estimation in OFDM systems. *2017 European Navigation Conference (ENC)*, Lausanne, Switzerland, 305–310. https://doi.org/10.1109/EURONAV.2017.7954222

Benedetto, F., Giunta, G., & Guzzon, E. (2011, April). Enhanced TOA-based indoor-positioning algorithm for mobile LTE cellular systems. *2011 8th Workshop on Positioning, Navigation and Communication*, Dresden, Germany, 137–142. https://doi.org/10.1109/WPNC.2011.5961030

Benedetto, F., Giunta, G., Toscano, A., & Vegni, L. (2007, April). Dynamic LOS/NLOS statistical discrimination of wireless mobile channels. *2007 IEEE 65th Vehicular Technology Conference-VTC2007-Spring*, Dublin, Ireland, 3071–3075. https://doi.org/10.1109/VETECS.2007.629

Chen, C. Y., & Wu, W. R. (2016). Three-dimensional positioning for LTE systems. *IEEE Transactions on Vehicular Technology*, *66*(4), 3220–3234. https://doi.org/10.1109/TVT.2016.2593697

Chen, J., Yin, X., Tian, L., Zhang, N., He, Y., Cheng, X., Duan, W., & Ruiz Boqué, S. (2014). Measurement-based LoS/NLoS channel modeling for hot-spot urban scenarios in UMTS networks. *International Journal of Antennas and Propagation*, *2014*(454976), 1–12. https://doi.org/10.1155/2014/454976

Cherian, S. S., & Rudrapatna, A. N. (2013). LTE location technologies and delivery solutions. *Bell Labs Technical Journal*, *18*(2), 175–194. https://doi.org/10.1002/bltj.21612

Dammann, A., Staudinger, E., Sand, S., Gentner, C., & Wang, W. (2011, September). Joint GNSS and 3GPP-LTE based positioning in outdoor-to-indoor environments - performance evaluation and verification. *Proceedings of the 24th International Technical*

Meeting of the Satellite Division of The Institute of Navigation (ION GNSS 2011), Portland, OR, 3587–3595. https://www.ion.org/publications/abstract.cfm?articleID=9912

Dan, Z., Lian, B., & Xu, H. (2018, September). Research on LTE positioning algorithm under multipath environment. *2018 IEEE International Conference on Signal Processing, Communications and Computing (ICSPCC)*, Qingdao, China, 1–6. https://doi.org/10.1109/ICSPCC.2018.8567820

Dardari, D., Chong, C., & Win, M. Z. (2008). Threshold-based time-of-arrival estimators in UWB dense multipath channels. *IEEE Transactions on Communications*, *56*(8), 1366–1378. https://doi.org/10.1109/TCOMM.2008.050551

del Peral-Rosado, J. A., Castillo, R. E. I., Mıguez-Sánchez, J., Navarro-Gallardo, M., Garcıa-Molina, J. A., López-Salcedo, J. A., … Crisci, M. (2016, December). Performance analysis of hybrid GNSS and LTE localization in urban scenarios. *2016 8th ESA Workshop on Satellite Navigation Technologies and European Workshop on GNSS Signals and Signal Processing (NAVITEC)*, Noordwijk, The Netherlands, 1–8. https://doi.org/10.1109/NAVITEC.2016.7849332

del Peral-Rosado, J. A., López-Salcedo, J. A., Seco-Granados, G., Zanier, F., & Crisci, M. (2012a, September). Analysis of positioning capabilities of 3GPP LTE. *Proceedings of the 25th International Technical Meeting of the Satellite Division of The Institute of Navigation (ION GNSS 2012)*, Nashville, TN, 650–659.

del Peral-Rosado, J. A., López-Salcedo, J. A., Seco-Granados, G., Zanier, F., & Crisci, M. (2012b, June). Achievable localization accuracy of the positioning reference signal of 3GPP LTE. *2012 International Conference on Localization and GNSS*, Starnberg, Germany, 1–6. https://doi.org/10.1109/ICL-GNSS.2012.6253127

del Peral-Rosado, J. A., López-Salcedo, J. A., Seco-Granados, G., Zanier, F., & Crisci, M. (2012c, September). Evaluation of the LTE positioning capabilities under typical multipath channels. *2012 6th Advanced Satellite Multimedia Systems Conference (ASMS) and 12th Signal Processing for Space Communications Workshop (SPSC)*, Baiona, Spain, 139–146. https://doi.org/10.1109/ASMS-SPSC.2012.6333065

del Peral-Rosado, J. A., López-Salcedo, J. A., Seco-Granados, G., Zanier, F., & Crisci, M. (2014). Joint maximum likelihood time-delay estimation for LTE positioning in multipath channels. *EURASIP Journal on Advances in Signal Processing*, *2014*(1), 33. https://doi.org/10.1186/1687-6180-2014-33

del Peral-Rosado, J. A., López-Salcedo, J. A., Seco-Granados, G., Zanier, F., Crosta, P., Ioannides, R., & Crisci, M. (2013, October). Software-defined radio LTE positioning receiver towards future hybrid localization systems. *31st AIAA International Communications Satellite Systems Conference 2013*, Florence, Italy. https://doi.org/10.2514/6.2013-5610

del Peral-Rosado, J. A., López-Salcedo, J. A., Zanier, F., & Seco-Granados, G. (2018). Position accuracy of joint time-delay and channel estimators in LTE networks. *IEEE Access*, *6*, 25185–25199. https://doi.org/10.1109/ACCESS.2018.2827921

del Peral-Rosado, J. A., Parro-Jiménez, J. M., López-Salcedo, J. A., Seco-Granados, G., Crosta, P., Zanier, F., & Crisci, M. (2014, December). Comparative results analysis on positioning with real LTE signals and low-cost hardware platforms. *2014 7th ESA Workshop on Satellite Navigation Technologies and European Workshop on GNSS Signals and Signal Processing (NAVITEC)*, Noordwijk, The Netherlands, 1–8. https://doi.org/10.1109/NAVITEC.2014.7045148

del Peral-Rosado, J. A., Raulefs, R., López-Salcedo, J. A., & Seco-Granados, G. (2017). Survey of cellular mobile radio localization methods: From 1G to 5G. *IEEE Communication Surveys and Tutorials*, *20*(2), 1124–1148. https://doi.org/10.1109/COMST.2017.2785181

Driusso, M. (2016). *Time of arrival estimation of LTE signals for positioning: Bounds and algorithms* (Doctoral dissertation, University of Trieste). https://arts.units.it/retrieve/handle/11368/2908081/187289/phd_thesis.pdf

Driusso, M., Comisso, M., Babich, F., & Marshall, C. (2014). Performance analysis of time of arrival estimation on OFDM signals. *IEEE Signal Processing Letters*, *22*(7), 983–987. https://doi.org/10.1109/LSP.2014.2378994

Driusso, M., Marshall, C., Sabathy, M., Knutti, F., Mathis, H., & Babich, F. (2016, October). Indoor positioning using LTE signals. *2016 International Conference on Indoor Positioning and Indoor Navigation (IPIN)*, Madrid, Spain, 1–8. https://doi.org/10.1109/IPIN.2016.7743656

Driusso, M., Marshall, C., Sabathy, M., Knutti, F., Mathis, H., & Babich, F. (2017). Vehicular position tracking using LTE signals. *IEEE Transactions on Vehicular Technology*, *66*(4), 3376–3391. https://doi.org/10.1109/TVT.2016.2589463

Gadka, P., Sadowski, J., & Stefanski, J. (2019). Detection of the first component of the received LTE signal in the OTDoA method. *Wireless Communications and Mobile Computing*, *2019*, 1–12. https://doi.org/10.1155/2019/2708684

Gentner, C., Muñoz, E., Khider, M., Staudinger, E., Sand, S., & Dammann, A. (2012, April). Particle filter based positioning with 3GPP-LTE in indoor environments. *Proceedings of the 2012 IEEE/ION Position, Location and Navigation Symposium*, Myrtle Beach, SC, 301–308. https://doi.org/10.1109/PLANS.2012.6236895

Gentner, C., Sand, S., & Dammann, A. (2012, June). OFDM indoor positioning based on TDOAs: Performance analysis and experimental results. *2012 International Conference on Localization and GNSS*, Starnberg, Germany, 1–7. https://doi.org/10.1109/ICL-GNSS.2012.6253136

Giorgetti, A., & Chiani, M. (2013). Time-of-arrival estimation based on information theoretic criteria. *IEEE Transactions on Signal Processing*, *61*(8), 1869–1879. https://doi.org/10.1109/TSP.2013.2239643

Guvenc, I., & Sahinoglu, Z. (2005, September). Threshold-based TOA estimation for impulse radio UWB systems. *2005 IEEE International Conference on Ultra-Wideband*, Zurich, Switzerland, 420–425. https://doi.org/10.1109/ICU.2005.1570024

Hu, S., Li, X., & Rusek, F. (2019, April). On time-of-arrival estimation in NB-IoT systems. *2019 IEEE Wireless Communications and Networking Conference (WCNC)*, Marrakesh, Morocco, 1–6. https://doi.org/10.1109/WCNC.2019.8885551

Huang, M., & Xu, W. (2013, April). Enhanced LTE TOA/OTDOA estimation with first arriving path detection. *2013 IEEE Wireless Communications and Networking Conference (WCNC)*, Shanghai, China, 3992–3997. https://doi.org/10.1109/WCNC.2013.6555215

Ikhtiari, N. (2019). *Navigation in GNSS denied environments using software defined radios and LTE signals of opportunities* (Master's thesis). University of Canterbury Research Repository.

Karisan, Y., Dardari, D., Gezici, S., D'Amico, A. A., & Mengali, U. (2011). Range estimation in multicarrier systems in the presence of interference: Performance limits and optimal signal design. *IEEE Transactions on Wireless Communications*, *10*(10), 3321–3331. https://doi.org/10.1109/TWC.2011.072511.101844

Knutti, F., Sabathy, M., Driusso, M., Mathis, H., & Marshall, C. (2015, April). Positioning using LTE signals. *Proceedings of Navigation Conference in Europe 2015*, Bordeaux, France, 1–8.

Kong, S. H., & Kim, B. (2016). Error analysis of the OTDOA from the resolved first arrival path in LTE. *IEEE Transactions on Wireless Communications*, *15*(10), 6598–6610. https://doi.org/10.1109/TWC.2016.2586469

Lee, J. Y., Choi, J. W., Lee, J. H., Yoon, J. M., & Kim, S. C. (2018). Enhanced path detection based on interference cancellation for range estimation of communication-based positioning system in indoor environment. *IEEE Access*, *7*, 1658–1667. https://doi.org/10.1109/ACCESS.2018.2886760

Li, X., & Pahlavan, K. (2004). Super-resolution TOA estimation with diversity for indoor geolocation. *IEEE Transactions on Wireless Communications*, *3*(1), 224–234. https://doi.org/10.1109/TWC.2003.819035

Liavas, A. P., Regalia, P. A., & Delmas, J. P. (1999). Blind channel approximation: Effective channel order determination. *IEEE Transactions on Signal Processing*, *47*(12), 3336–3344. https://doi.org/10.1109/78.806077

Liu, Y., Tan, Z., Hu, H., Cimini, L. J., & Li, G. Y. (2014). Channel estimation for OFDM. *IEEE Communication Surveys and Tutorials*, *16*(4), 1891–1908. https://doi.org/10.1109/COMST.2014.2320074

Luan, D. (2017). *Fundamental performance limits on time of arrival estimation accuracy with 5G radio access* (Degree project). KTH Royal Institute of Technology Publications Database.

Medbo, J., Siomina, I., Kangas, A., & Furuskog, J. (2009, September). Propagation channel impact on LTE positioning accuracy: A study based on real measurements of observed time difference of arrival. *2009 IEEE 20th International Symposium on Personal, Indoor and Mobile Radio Communications*, Tokyo, Japan, 2213–2217. https://doi.org/10.1109/PIMRC.2009.5450144

Mensing, C., Plass, S., & Dammann, A. (2007, March). Synchronization algorithms for positioning with OFDM communications signals. *2007 4th Workshop on Positioning, Navigation and Communication*, Hannover, Germany, 205–210. https://doi.org/10.1109/WPNC.2007.353635

Mensing, C., Sand, S., & Dammann, A. (2010). Hybrid data fusion and tracking for positioning with GNSS and 3GPP-LTE. *International Journal of Navigation and Observation*, *2010*(812945), 1–12. https://doi.org/10.1155/2010/812945

Mensing, C., Sand, S., Dammann, A., & Utschick, W. (2009a, November). Data-aided location estimation in cellular OFDM communications systems. *2009 IEEE Global Telecommunications Conference*, Honolulu, HI, 1–7. https://doi.org/10.1109/GLOCOM.2009.5426060

Mensing, C., Sand, S., Dammann, A., & Utschick, W. (2009b, June). Interference-aware location estimation in cellular OFDM communications systems. *2009 IEEE International Conference on Communications*, Dresden, Germany, 1–6. https://doi.org/10.1109/ICC.2009.5199097

Müller, P., del Peral-Rosado, J. A., Piche, R., & Seco-Granados, G. (2016). Statistical trilateration with skew-t distributed errors in LTE networks. *IEEE Transactions on Wireless Communications*, *15*(10), 7114–7127. https://doi.org/10.1109/TWC.2016.2597836

Noschese, M., Babich, F., Comisso, M., & Marshall, C. (2018, September). On the performance of SAGE algorithm for ToA estimation in dual-band OFDM systems. *2018 IEEE 29th Annual International Symposium on Personal, Indoor and Mobile Radio Communications (PIMRC)*, Bologna, Italy, 1–6. https://doi.org/10.1109/PIMRC.2018.8580705

Noschese, M., Babich, F., Comisso, M., Marshall, C., & Driusso, M. (2017, August). A low-complexity approach for time of arrival estimation in OFDM systems. *2017 International Symposium on Wireless Communication Systems (ISWCS)*, Bologna, Italy, 128–133. https://doi.org/10.1109/ISWCS.2017.8108096

Panchetti, M., Carbonelli, C., Horvat, M., & Luise, M. (2013, March). Performance analysis of PRS-based synchronization algorithms for LTE positioning applications. *2013 10th Workshop on Positioning, Navigation and Communication (WPNC)*, Dresden, Germany, 1–6. https://doi.org/10.1109/WPNC.2013.6533292

Parkinson, B. W., Enge, P., Axelrad, P., & Spilker, Jr, J. J. (Eds.). (1996). *Global positioning system: Theory and applications* (Vol. II). American Institute of Aeronautics and Astronautics.

Pittino, F., Driusso, M., Dalla Torre, A., & Marshall, C. (2017, May). Outdoor and indoor experiments with localization using LTE signals. *2017 European Navigation Conference (ENC)*, Lausanne, Switzerland, 311–321. https://doi.org/10.1109/EURONAV.2017.7954223

Radnosrati, K., Hendeby, G., Fritsche, C., Gunnarsson, F., & Gustafsson, F. (2017, October). Performance of OTDOA positioning in narrowband IoT systems. *2017 IEEE 28th Annual International Symposium on Personal, Indoor, and Mobile Radio Communications (PIMRC)*, Quebec, Canada, 1–7. https://doi.org/10.1109/PIMRC.2017.8292365

Rydén, H., Razavi, S. M., Gunnarsson, F., Kim, S. M., Wang, M., Blankenship, Y., … Busin, Å. (2015, June). Baseline performance of LTE positioning in 3GPP 3D MIMO indoor user scenarios. *2015 International Conference on Location and GNSS (ICL-GNSS)*, Gothenburg, Sweden, 1–6. https://doi.org/10.1109/ICL-GNSS.2015.7217158

Rydén, H., Zaidi, A. A., Razavi, S. M., Gunnarsson, F., & Siomina, I. (2016, September). Enhanced time of arrival estimation and quantization for positioning in LTE networks. *2016 IEEE 27th Annual International Symposium on Personal, Indoor, and Mobile Radio Communications (PIMRC)*, Valencia, Spain, 1–6. https://doi.org/10.1109/PIMRC.2016.7794634

Saberinia, E., & Tewfik, A. H. (2008). Ranging in multiband ultra-wideband communication systems. *IEEE Transactions on Vehicular Technology*, *57*(4), 2523–2530. https://doi.org/10.1109/TVT.2007.904526

Shamaei, K., & Kassas, Z. M. (2018). LTE receiver design and multipath analysis for navigation in urban environments. *NAVIGATION*, *65*(4), 655–675. https://doi.org/10.1002/navi.272

Shamaei, K., Khalife, J., & Kassas, Z. M. (2017, January). Comparative results for positioning with secondary synchronization signal versus cell specific reference signal in LTE systems. *Proceedings of the 2017 International Technical Meeting of The Institute of Navigation*, Monterey, CA, 1256–1268. https://doi.org/10.33012/2017.14885

Shamaei, K., Khalife, J., & Kassas, Z. M. (2018a, April). Pseudorange and multipath analysis of positioning with LTE secondary synchronization signals. *2018 IEEE Wireless Communications and Networking Conference (WCNC)*, Barcelona, Spain, 1–6. https://doi.org/10.1109/WCNC.2018.8377438

Shamaei, K., Khalife, J., & Kassas, Z. M. (2018b). Exploiting LTE signals for navigation: Theory to implementation. *IEEE Transactions on Wireless Communications*, *17*(4), 2173–2189. https://doi.org/10.1109/TWC.2018.2789882

Staudinger, E., & Gentner, C. (2011, April). TDoA subsample delay estimator with multiple access interference mitigation and carrier frequency offset compensation for OFDM based systems. *2011 8th Workshop on Positioning, Navigation and Communication*, Dresden, Germany, 33–38. https://doi.org/10.1109/WPNC.2011.5961011

Staudinger, E., Klein, C., & Sand, S. (2011, May). A generic OFDM based TDoA positioning testbed with interference mitigation for subsample delay estimation. *2011 8th International Workshop on Multi-Carrier Systems & Solutions*, Herrsching, Germany, 1–5. https://doi.org/10.1109/MC-SS.2011.5910707

Sven, F. (2014). *Observed time difference of arrival (OTDOA) positioning in 3GPP LTE*. Qualcomm Technologies, Inc.

Torrieri, D. (2005). *Principles of spread-spectrum communication systems*. Springer.

Townsend, B. R., Fenton, P. C., Van Dierendonck, K. J., & Van Nee, D. R. (1995). Performance evaluation of the multipath estimating delay lock loop. *NAVIGATION*, *42*(3), 502–514. https://doi.org/10.1002/j.2161-4296.1995.tb01903.x

Ulmschneider, M., & Gentner, C. (2016, April). Multipath assisted positioning for pedestrians using LTE signals. *2016 IEEE/ION Position, Location and Navigation Symposium (PLANS)*, Savannah, GA, 386–392. https://doi.org/10.1109/PLANS.2016.7479725

Via, J., Santamaria, I., & Perez, J. (2006). Effective channel order estimation based on combined identification/equalization. *IEEE Transactions on Signal Processing*, *54*(9), 3518–3526. https://doi.org/10.1109/TSP.2006.879271

Wang, D., & Fattouche, M. (2010). OFDM transmission for time-based range estimation. *IEEE Signal Processing Letters*, *17*(6), 571–574. https://doi.org/10.1109/LSP.2010.2047958

Wang, P., & Morton, Y. T. (2020). Multipath estimating delay lock loop for LTE signal TOA estimation in urban and indoor environments. *IEEE Transactions on Wireless Communications*, *19*(8), 5518–5530. https://doi.org/10.1109/TWC.2020.2994037

Wang, T., Shen, Y., Mazuelas, S., Shin, H., & Win, M. Z. (2013). On OFDM ranging accuracy in multipath channels. *IEEE Systems Journal*, *8*(1), 104–114. https://doi.org/10.1109/JSYST.2013.2260640

Wang, W., Jost, T., Gentner, C., Zhang, S., & Dammann, A. (2015). A semiblind tracking algorithm for joint communication and ranging with OFDM signals. *IEEE Transactions on Vehicular Technology*, *65*(7), 5237–5250. https://doi.org/10.1109/TVT.2015.2468079

Xu, H., Chong, C. C., Guvenc, I., Watanabe, F., & Yang, L. (2008, May). High-resolution TOA estimation with multi-band OFDM UWB signals. *2008 IEEE International Conference on Communications*, Beijing, China, 4191–4196. https://doi.org/10.1109/ICC.2008.787

Xu, W., Huang, M., Zhu, C., & Dammann, A. (2016). Maximum likelihood TOA and OTDOA estimation with first arriving path detection for 3GPP LTE system. *Transactions on Emerging Telecommunications Technologies*, *27*(3), 339–356. https://doi.org/10.1002/ett.2871

Yang, B., Letaief, K. B., Cheng, R. S., & Cao, Z. (2000). Timing recovery for OFDM transmission. *IEEE Journal on Selected Areas in Communications*, *18*(11), 2278–2291. https://doi.org/10.1109/49.895033

Yang, J., Wang, X., Park, S. I., & Kim, H. M. (2012). Direct path detection using multipath interference cancelation for communication-based positioning system. *EURASIP Journal on Advances in Signal Processing*, *2012*(1), 188. https://doi.org/10.1186/1687-6180-2012-188

How to cite this article: Wang P, Morton YJ. Performance comparison of time-of-arrival estimation techniques for LTE signals in realistic multipath propagation channels. *NAVIGATION*. 2020;67:691–712. https://doi.org/10.1002/navi.395

APPENDIX

This appendix provides some representative simulation results to clarify the parameter selection process for the FPD technique.

Figure A1 shows the RMS values of the TOA estimation errors obtained with the FPD technique based on threshold criterion 1 as a function of the normalized threshold (T_{norm}) for three channel models and two SNR values when $N_{\text{RB}} = 100$. As can be observed, for all the considered normalized threshold values, the optimal one leading to the lowest RMS depends on both the SNR condition and channel type. For example, the optimal T_{norm} is 0.6 for the EPA model when SNR $= -10$ dB, while it is 0.1 for the ETU model when SNR $= 0$ dB. Overall, $T_{\text{norm}} = 0.4$ is a good choice for all the considered simulation conditions.

Figure A2 plots the RMS values of the TOA estimation errors and the number of TOA estimations obtained with the FPD technique based on threshold criterion 2 as a function of the early detection probability (P_{ed}). Three channel models and two SNR values are taken into consideration, and N_{RB} is set to 100. Figure A2 indicates that the FPD technique based on threshold criterion 2 can always generate TOA estimations for high SNR conditions, and thus a smaller early detection probability is preferable for obtaining a lower RMS value. While for low SNR values, a higher early detection probability should be used to improve the measurement availability and also the estimation accuracy. As can be seen, $P_{\text{ed}} = 10^{-6}$ is a reasonable choice for different simulation conditions.

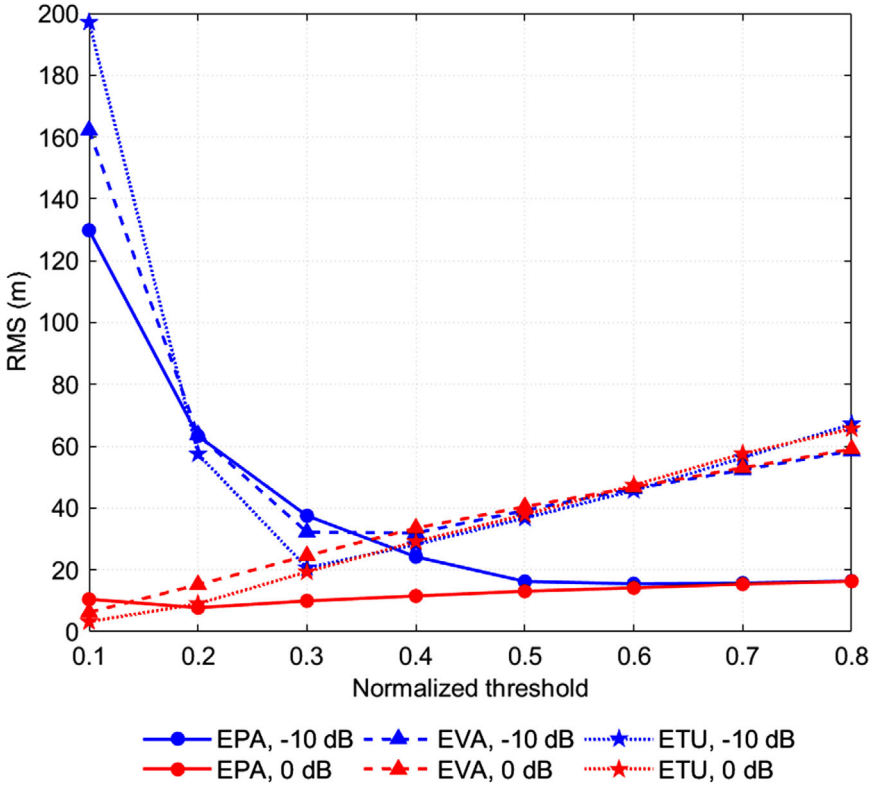

FIGURE A1 RMS of the TOA estimation errors versus normalized threshold provided by the FPD technique based on threshold criterion 1 for three channel models and two SNR values when $\boldsymbol{N}_{\mathbf{RB}} = 100$ [Color figure can be viewed in the online issue, which is available at wileyonlinelibrary.com and www.ion.org]

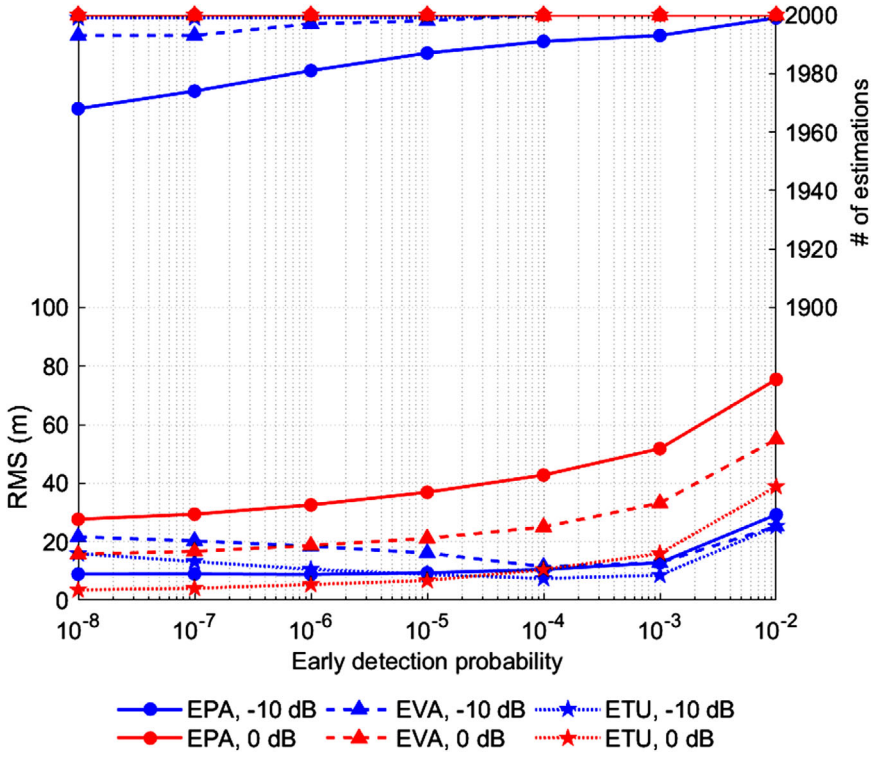

FIGURE A2 RMS of the TOA estimation errors and number of the TOA estimations versus early detection probability provided by FPD technique based on threshold criterion 2 for three channel models and two SNR values when $\boldsymbol{N}_{\mathbf{RB}} = 100$ [Color figure can be viewed in the online issue, which is available at wileyonlinelibrary.com and www.ion.org]